

Ostwald ripening of droplets: The role of migration

KARL GLASNER¹, FELIX OTTO², TOBIAS RUMP²
AND DEJAN SLEPČEV³

¹University of Arizona, 617 N. Santa Rita, Tucson, AZ 85721, U.S.A.
email: kglasner@math.arizona.edu

²University of Bonn, Wegelerstraße 10, D–53115 Bonn, Germany
email: otto@iam.uni-bonn.de; rump@iam.uni-bonn.de

³Carnegie Mellon University, Pittsburgh, PA 15213-3890, U.S.A.
email: slepcev@math.cmu.edu

(Received 14 June 2007; revised 20 March 2008; first published online 2 June 2008)

A configuration of near-equilibrium liquid droplets sitting on a precursor film which wets the entire substrate can coarsen in time by two different mechanisms: *collapse* or *collision* of droplets. The collapse mechanism, i.e., a larger droplet grows at the expense of a smaller one by mass exchange through the precursor film, is also known as Ostwald ripening. As was shown by K. B. Glasner and T. P. Witelski ('Collision versus collapse of droplets in coarsening of dewetting thin films', *Phys. D* **209**(1–4), 2005, 80–104) in case of a one-dimensional substrate, the migration of droplets may interfere with Ostwald ripening: The configuration can coarsen by collision rather than by collapse. We study the role of migration in case of a two-dimensional substrate for a whole range of mobilities. We characterize the velocity of a single droplet immersed into an environment with constant flux field far away. This allows us to describe the dynamics of a droplet configuration on a two-dimensional substrate by a system of ODEs. In particular, we find by heuristic arguments that collision can be a relevant coarsening mechanism.

1 Introduction

We are interested in the coarsening dynamics of a configuration of near-equilibrium liquid droplets sitting on a flat precursor film which wets the entire substrate (see Figure 1). By coarsening we mean in particular the decrease of the number of droplets in time. The dynamics of the coarsening process is driven by the reduction of total energy.

The coarsening process can be mediated by two mechanisms: *collapse* and *collision* of droplets. Collapse relies on the mass exchange between droplets through the precursor layer (see Figure 2). This process is also known as Ostwald ripening. Collisions of droplets can happen due to the motion of droplets on the precursor layer (see Figure 3). (For a more detailed discussion of the underlying physics we refer to the introduction of [13].)

Traditional Ostwald ripening in binary mixtures, as described by the Cahn–Hilliard equation, is well understood. A sparse configuration of spherically symmetric particles

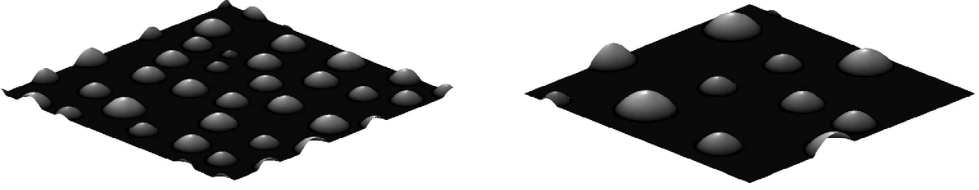


FIGURE 1. A typical configuration of droplets connected by a uniform precursor layer on a two-dimensional substrate at two different times.

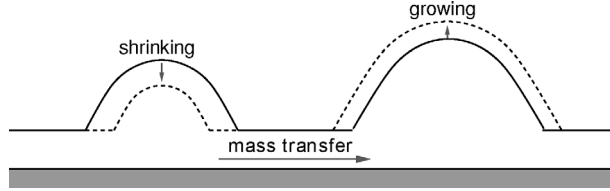


FIGURE 2. Collapse mechanism: A pressure gradient is responsible for the mass transfer through the connecting film. Eventually, the smaller droplet vanishes.

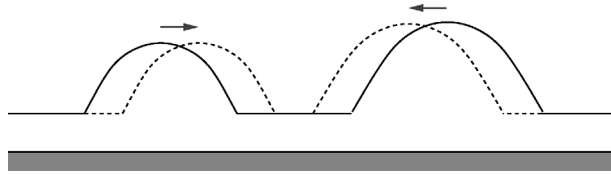


FIGURE 3. Collision mechanism: Droplets migrate on the film which can lead to coarsening. (The illustration is in the reference frame with fixed center of mass.)

of the minority phase immersed into a matrix of the majority phase will age over time: The large particles grow at the expense of smaller ones which eventually disappear; the configuration coarsens over time. A flux across the matrix allows for the mass exchange between the particles. Migration of the particles opposite to the dominant direction of the ambient flux is a much slower process and does not affect Ostwald ripening in the low volume-fraction regime. In the sharp-interface limit, the Mullins–Sekerka free boundary problem, the ripening dynamics of particles were studied analytically in [2] and [3].

Our physical system differs from binary mixtures in two respects. The first, obvious, difference lies in a ‘mixed dimensionality’: Kinetics (the mass exchange between the droplets) is governed by flux through the precursor film on the d -dimensional substrate ($d = 1$ and $d = 2$ being physically relevant) as in binary mixtures. Energetics however is $(d + 1)$ -dimensional in the sense that the surface tension corresponds to the surface of a $(d + 1)$ -dimensional droplet (while the interfacial energy in binary mixtures corresponds to the surface of a d -dimensional particle). The second, more subtle, difference comes from the variable mobility in the thin-film equation: Since the mobility strongly increases with height (see (1.3)), large droplets are, relatively speaking, much more mobile than large particles.

The role of migration of droplets on a one-dimensional substrate in the long-time dynamics is studied by Glasner and Witelski in [9]. They identify regimes in terms of the precursor height and the average film height where each of the coarsening mechanism is dominant. In [15], Pismen and Pomeau derive, assuming quasi-stationarity of the system, an equation for the droplet motion in an interacting system. We obtain qualitatively different results. These differences are discussed at length in Appendix C, and analytical justification for the noted disparities are highlighted.

In [13], we studied the statistical behaviour of the dynamics characterized by a single coarsening exponent and established an upper bound on the coarsening rate. Let us state that our rigorous result was independent of the question whether migration or Ostwald ripening is the dominant mechanism.

The purpose of this paper is to study the role of migration for the coarsening process in terms of the variable mobility in the thin-film equation. We gain the following insights:

- A single droplet in an ambient flux field migrates in the direction of the flux source, i.e. the migration velocity is antiparallel to the flux field (see Figure 6).
- The interplay between Ostwald ripening and migration in a many-droplet system is as follows: The ripening generates an ambient flux field which affects the droplet migration as in the single-droplet case. Vice versa, migration changes the locations of the droplets from which the flux stems.
- The migration velocity and the volume change can be quantified in terms of scaling in the droplet size and distance which yield heuristically the typical time scales for migration and Ostwald ripening. The scaling laws depend on the mobility and the average film height.
- Collision of migrating droplets generically occurs for a configuration of two relatively small droplets submerged into a matrix of larger droplets. Therefore, the time scales for migration and Ostwald ripening heuristically yield the relative importance of collisions for the coarsening process. In particular, we find that for $q \geq 3$ and large average film height the coarsening process of a droplet configuration is collision-dominated.

The *outline* of this paper is as follows: The remainder of this section is devoted to the derivation of the thin-film equation. In Section 2, we review the derivation of the equilibrium droplet profile. The ‘model problem’, that is, a single near-equilibrium droplet in an ambient flux field, is studied in Section 3 where we characterize the migration velocity (formula (3.24)). For readability, we have left the detailed analysis of auxiliary functions related to this section to Appendices A and B. The interaction of droplets in a reduced configuration space is analysed in Section 4 by means of the Rayleigh principle. The evolution of the system is described by the system of ODEs (4.13), whose coefficients are investigated in Subsection 4.2. In the case of two interacting droplets the system is also presented in an explicit form in (4.25) and (4.26). Time scales of the dynamics are investigated in Subsection 4.2.2. In Appendix C we present the analysis of a related problem of a single droplet sliding due to external potential (for example due to gravitation on an inclined substrate). For comparison with Sections 3 and 4, in Appendix D we present the analysis in one-dimensional setting. In Appendix E we present numerical experiments which not only confirm some of our findings, but also help

visualize the dynamics. In Appendix F we compare the approach of this paper to a more standard approach via matched asymptotic expansion.

The results in Section 3 rely on the assumption that the system is quasi-stationary. The results of Section 4 are carried out on the level of the model problem, which encodes the quasi-stationary nature of the system. Proving the results rigorously remains an open problem. Let us note that while the system is similar to the Cahn–Hilliard equation the approach to deriving the equations for the motion of droplets is somewhat different. Namely, for the Cahn–Hilliard equation one first considers an intermediate system: the sharp-interface dynamics given by the Mullins–Sekerka equation. Then the equations for evolution of ‘droplets’ are derived from the Mullins–Sekerka equation. In the case of the Cahn–Hilliard equation there are rigorous results in this direction, for the first step by Alikakos, Bates and Chen [1], and for the derivation of approximating ODE system by Alikakos and Fusco [2], and Alikakos Fusco and Karali [4].

1.1 Kinematics, kinetics and energetics

1.1.1 Kinematics

In the thin-film approximation, the state of the system at time t is described by the film height $h = h(x, t) > 0$ over a point $x \in \mathbb{R}^d$ on the substrate. Conservation of mass assumes the form of a continuity equation for h :

$$\partial_t h + \nabla \cdot J = 0, \quad (1.1)$$

where the volume flux $J = J(x, t) \in \mathbb{R}^d$ is a vector field of the substrate dimension d .

1.1.2 Kinetics

In the thin-film approximation, the flux is generated by the gradient of the pressure μ

$$J = -m(h) \nabla \mu, \quad (1.2)$$

where the mobility m is a function of h . The form of the mobility–height relation depends on the underlying $(d + 1)$ -dimensional fluid model which specifies in particular the boundary condition for the fluid velocity at the substrate. For the Stokes equation with no-slip boundary condition, one obtains in the thin-film approximation after suitable non-dimensionalization [12]

$$m(h) = h^3.$$

For the Stokes equation with a Navier slip-condition [10], the mobility is less degenerate:

$$m(h) = h^2 \quad \text{as long as } h \ll \text{slippage length.}$$

In case of Darcy’s equation [5] with no-flux boundary conditions, one ends up with

$$m(h) = h.$$

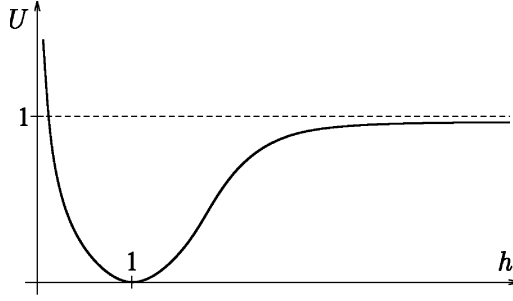


FIGURE 4. Short-range interaction potential.

In order to capture the effect of different kinetics, it is convenient to study all homogeneous mobility functions at once:

$$m(h) = h^q \quad \text{for some fixed } q \geq 0. \quad (1.3)$$

1.1.3 Energetics

We envision a thermodynamically driven situation, where the pressure comes in form of the functional derivative of a free energy E in the film height:

$$\mu = \frac{\delta E}{\delta h}. \quad (1.4)$$

In our case, the energy is the sum of the surface energy between liquid and vapour and a short-range interaction potential between substrate, liquid film and vapour (which is only effective where h is sufficiently small):

$$E(h) = \int \frac{1}{2} |\nabla h|^2 + U(h) dx, \quad (1.5)$$

where a typical model (see [17] for example) for the short-range potential is

$$U(h) = \frac{\beta}{\alpha - \beta} h^{-\alpha} - \frac{\alpha}{\alpha - \beta} h^{-\beta} + 1 \quad \text{for some } 0 < \beta < \alpha; \quad (1.6)$$

See Figure 4. The potential is normalized by

$$\lim_{h \uparrow \infty} U = 1.$$

Moreover, we have non-dimensionalized horizontal length x and height h such that

$$\min_h U = U(h = 1) = 0. \quad (1.7)$$

Note that in case of (1.5),

$$\mu = -\Delta h + U'(h), \quad (1.8)$$

where the prime stands for the ordinary derivative w.r.t. the variable h .

1.2 Gradient flow structure and Rayleigh principle

Combining (1.1), (1.2), (1.4) and (1.8), one obtains a non-linear fourth-order parabolic equation for h :

$$\partial_t h - \nabla \cdot (m(h)\nabla(-\Delta h + U'(h))) = 0. \quad (1.9)$$

Mathematically speaking, (1.9) is a variant of the Cahn–Hilliard equation if one interprets h as the conserved order parameter. The difference from the standard Cahn–Hilliard equation is both in energetics and kinetics. The difference in energetics is that the nonconvex potential U is not a ‘double-well potential’ of the universal Ginzburg–Landau type: It only has a single *finite* minimum (even when shifted by a linear function). However, the other minimum can be thought of as $h = +\infty$. The difference in kinetics lies in the fact that the mobility m strongly depends on the order parameter. Of course, solution-dependent and even degenerate mobilities have been considered in the context of the Cahn–Hilliard (see [6] for a mathematical treatment). But the power-law dependence (1.3) together with the fact that the range of h -values is infinite gives rise to new phenomena.

Not surprisingly in view of its derivation, the evolution defined through (1.9) has the mathematical structure of a gradient flow – irrespective of the particular form (1.3) of the mobility function or the energy (1.5). From a more traditional point of view this means that there is a Rayleigh principle (see [11] and references therein): At any time the flux J minimizes

$$\frac{1}{2} \times \text{dissipation rate } D + \text{infinitesimal change in energy } \dot{E}.$$

We note that the viscous dissipation rate is given by

$$D = \int \frac{1}{m(h)} |J|^2 dx$$

and according to (1.1) and (1.4), a flux J entails the infinitesimal change in energy

$$\dot{E} = \int \frac{\delta E}{\delta h} \partial_t h dx = \int \mu (-\nabla \cdot J) dx = \int \nabla \mu \cdot J dx.$$

Thus at any time, the flux is determined as the minimizer of the Rayleigh functional

$$\frac{1}{2} \int \frac{1}{m(h)} |J|^2 dx + \int J \cdot \nabla \mu dx = \frac{1}{2} \int \frac{1}{m(h)} |J|^2 dx + \int J \cdot \nabla (-\Delta h + U'(h)) dx.$$

One advantage of this formulation is that it separates kinetics (as highlighted by the mobility function $m(h)$) from energetics (as exemplified by the short-range potential $U(h)$). It uncovers the competition between driving thermodynamics and limiting viscous friction.

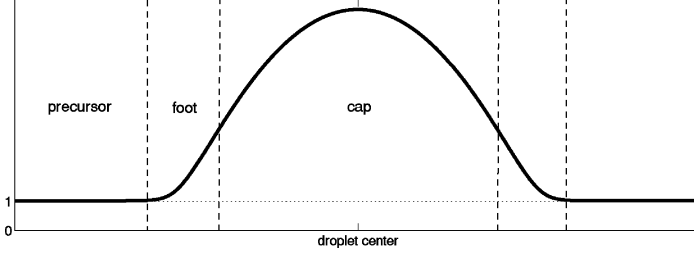


FIGURE 5. Cross section of an equilibrium droplet.

An immediate consequence of this variational principle is that the minimizer adjusts itself so that energy balance holds:

$$\dot{E} + D = 0.$$

Furthermore, the formulation based on Rayleigh principle enables us to effortlessly incorporate the systems with prescribed ‘far field’ flux (needed in Section 3) which do not conserve mass.

2 Equilibrium droplet

An equilibrium droplet (Figure 5) is a stationary point of the energy functional (1.5) subject to the constraint of constant volume $\int h dx$. In view of (1.4) and (1.8), this means that the pressure is constant:

$$\mu = -\Delta h + U'(h) = \text{const} =: P.$$

We are interested in radially symmetric equilibrium droplets \bar{h} of asymptotically constant height \bar{h}_∞ for $r = |x - X| \uparrow \infty$. We focus on the case of a two-dimensional substrate – the one-dimensional substrate is easier. In this case, equilibrium droplets are characterized as solutions of the ODE

$$\begin{aligned} -\partial_r^2 \bar{h} - r^{-1} \partial_r \bar{h} + U'(\bar{h}) &= P, \\ \partial_r \bar{h}(r=0) &= 0 \quad \text{and} \quad \lim_{r \uparrow \infty} \bar{h} = \bar{h}_\infty. \end{aligned} \tag{2.1}$$

Then necessarily $U'(\bar{h}_\infty) = P$.

We are interested in the regime where $0 < P \ll 1$ and $\bar{h}_\infty \approx 1$. We note that to leading order,

$$\bar{h}_\infty - 1 \approx \frac{1}{U''(1)} P \ll 1 \tag{2.2}$$

and thus in particular

$$U''(\bar{h}_\infty) \approx U''(1) > 0. \tag{2.3}$$

We now argue that the droplet profile satisfies

$$\bar{h} > \bar{h}_\infty \quad \text{and} \quad \partial_r \bar{h} < 0 \quad \text{for } r > 0. \tag{2.4}$$

Indeed, the ODE (2.1) can be interpreted as describing the ‘position’ \bar{h} as function of ‘time’ r of a particle in the potential $V(h) := -(U(h) - Ph)$ with inertia and friction:

$$\partial_r^2 \bar{h} + V'(\bar{h}) = -r^{-1} \partial_r \bar{h}.$$

Initially, the particle is at rest: $\partial_r \bar{h}(r = 0) = 0$. Asymptotically, it reaches \bar{h}_∞ , which is a local maximum of the potential V (cf. (2.3)). In view of (1.6), the potential satisfies:

$$\begin{aligned} \bar{h}_\infty \text{ is the only local maximum of } V, \\ \lim_{h \downarrow 0} V = -\infty, \quad \text{and} \quad \lim_{h \uparrow \infty} V = +\infty. \end{aligned}$$

Hence the height must stay above its asymptotic position, which proves the first item in (2.4). Furthermore, the particle can only come to rest in finite time on an uphill slope. But then it would be trapped below this V -value and could not reach the local maximum \bar{h}_∞ . This shows that the particle moves monotonically. More precisely $h_r < 0$ which establishes (2.4).

2.1 Precursor, foot and cap region of a droplet

For the convenience of the reader, we present the asymptotic analysis of the solution to (2.1) in the regime $P \ll 1$. It is similar to the one in [8]. This will also allow us to refer to some of the arguments and intermediate results later on. In view of (2.4), there exists a unique radius $R > 0$ such that

$$\bar{h}(r = R) = 2, \tag{2.5}$$

which we think of as the droplet radius.

Precursor region. We first consider the precursor region $r \geq R$. Let us neglect the first-order term in (2.1):

$$-\partial_r^2 \bar{h} + U'(\bar{h}) - U'(\bar{h}_\infty) = 0 \quad \text{for } r \geq R,$$

and check later that this is to leading order consistent. Because of the boundary condition in (2.1), we conclude from the above

$$-\frac{1}{2}(\partial_r \bar{h})^2 + W(\bar{h}) = 0 \quad \text{for } r \geq R, \tag{2.6}$$

where

$$W(h) := U(h) - (U(\bar{h}_\infty) + U'(\bar{h}_\infty)(h - \bar{h}_\infty)). \tag{2.7}$$

From (2.4), (2.5) and (2.6) we obtain

$$\int_{\bar{h}(r)}^2 \frac{1}{\sqrt{2W(h)}} dh = r - R. \tag{2.8}$$

Since

$$W(h) \approx \frac{1}{2} U''(\bar{h}_\infty) (h - \bar{h}_\infty)^2 \approx \frac{1}{2} U''(1) (h - \bar{h}_\infty)^2, \quad (2.9)$$

the integral in (2.8) diverges logarithmically near $h = \bar{h}_\infty$. Hence we have to leading order

$$\ln(\bar{h}(r) - \bar{h}_\infty) = \sqrt{U''(1)} (R - r) \quad \text{for } r - R \gg 1. \quad (2.10)$$

Thus the droplet height converges exponentially (at order-one rate) to its limiting value as the distance to the droplet perimeter increases.

The first-order term $\frac{1}{r} \partial_r \bar{h}$ is indeed negligible with respect to $U'(\bar{h}) - U'(\bar{h}_\infty) = W'(\bar{h})$. In view of (2.6), this follows from

$$\frac{1}{R} \sqrt{2W(h)} \ll W'(h) \quad \text{for all } \bar{h}_\infty \leq h \leq 2. \quad (2.11)$$

For h close to \bar{h}_∞ , both terms scale as $h - \bar{h}_\infty$ (cf. (2.9)). Thus (2.11) is satisfied provided $R \gg 1$. In the end, we shall see that $R \sim P^{-1}$ so that this is satisfied.

Foot region. It is convenient to introduce the change of variable

$$\frac{r}{R} = \exp\left(\frac{s}{R}\right) \quad (2.12)$$

for which (2.1) turns into

$$-\partial_s^2 \bar{h} + \exp\left(2\frac{s}{R}\right) (U'(\bar{h}) - U'(\bar{h}_\infty)) = 0 \quad \text{for } s \in \mathbb{R}.$$

For

$$\left|\frac{s}{R}\right| \ll 1 \iff \left|\frac{r}{R} - 1\right| \ll 1, \quad (2.13)$$

this equation is to leading order approximated by the autonomous equation

$$-\partial_s^2 \bar{h} + (U'(\bar{h}) - U'(\bar{h}_\infty)) = 0 \quad \text{for } \left|\frac{s}{R}\right| \ll 1.$$

This implies in original variables to leading order

$$-\frac{1}{2} (\partial_r \bar{h})^2 + W(\bar{h}) = \text{const} \quad \text{for } \left|\frac{r}{R} - 1\right| \ll 1. \quad (2.14)$$

Matching function and derivative of (2.6) and (2.14) in the overlap region $0 < r - R \ll R$, we gather that to leading order, the constant in (2.14) must vanish so that in view of (2.5) we have

$$\int_{\bar{h}(r)}^2 \frac{1}{\sqrt{2W(h)}} dh = r - R \quad \text{for } \left|\frac{r}{R} - 1\right| \ll 1. \quad (2.15)$$

From

$$W(h) \approx 1 \quad \text{for } 1 \ll h \ll P^{-1},$$

and (2.15) we deduce that to leading order

$$\bar{h}(r) = \sqrt{2}(R-r) \quad \text{for } 1 \ll R-r \ll \min\{R, P^{-1}\}. \quad (2.16)$$

Cap region. We preliminarily define the cap region as the region where

$$\bar{h} \gg 1 \quad \text{and} \quad U'(\bar{h}) \ll P. \quad (2.17)$$

Based on the form (1.6) of U , (2.17) is equivalent to

$$\bar{h} \gg (P^{-1})^{\frac{1}{\beta+1}}. \quad (2.18)$$

Because of (2.17), (2.1) is well approximated by

$$-\partial_r^2 \bar{h} - \frac{1}{r} \partial_r \bar{h} = P.$$

Taking into account the left boundary condition in (2.1), all solutions are of the form

$$\bar{h} = \bar{h}(r=0) - \frac{P}{4} r^2. \quad (2.19)$$

Matching function and derivative of (2.16) and (2.19) yields to leading order

$$P \approx \frac{2\sqrt{2}}{R} \quad \text{and} \quad \bar{h}(r=0) = \frac{R}{\sqrt{2}}. \quad (2.20)$$

Hence in view of (2.18) the cap region is characterized by

$$\bar{h} = \frac{R}{\sqrt{2}} \left(1 - \left(\frac{r}{R} \right)^2 \right) \quad \text{for } R-r \gg (P^{-1})^{\frac{1}{\beta+1}}. \quad (2.21)$$

Notice that in the overlap region $(P^{-1})^{\frac{1}{\beta+1}} \ll R-r \ll P^{-1}$, which is non-trivial because of $\beta > 0$, the functions (2.16) and (2.21) including their derivatives indeed agree to leading order.

Mesoscopic droplet profile. From the above analysis, we learn that there exists an R such that to leading order

$$R \approx 2\sqrt{2}P^{-1}, \quad (2.22)$$

$$\bar{h} = \frac{R}{\sqrt{2}} \left(1 - \left(\frac{r}{R} \right)^2 \right) \quad \text{for } R-r \gg 1, \quad (2.23)$$

$$\bar{h} = 1 \quad \text{for } r-R \gg 1. \quad (2.24)$$

Indeed, (2.22) is a reformulation of the first item in (2.20), (2.23) follows from the combination of (2.16) and (2.21), whereas (2.24) is a weakening of (2.10). Thus on a

mesoscopic level, \bar{h} is well described by what we call the mesoscopic droplet profile

$$\bar{h}_{\text{meso}} = \begin{cases} \frac{R}{\sqrt{2}} \left(1 - \left(\frac{r}{R} \right)^2 \right) + 1 & \text{for } r \leq R, \\ 1 & \text{for } r \geq R \end{cases} \quad \text{where } R = 2\sqrt{2}P^{-1}. \quad (2.25)$$

This is not surprising, since \bar{h}_{meso} is the radially symmetric minimizer of the mesoscopic energy functional

$$E_{\text{meso}}(h) = \int \frac{1}{2} |\nabla h|^2 + U_{\text{meso}}(h) dx \quad (2.26)$$

where

$$U_{\text{meso}}(h) = \begin{cases} 1 & \text{for } h > 1, \\ 0 & \text{for } h \leq 1. \end{cases} \quad (2.27)$$

In particular, the apparent contact angle corresponds to a slope of $\sqrt{2}$ in our non-dimensionalization (1.7).

3 Droplet migration

In this section, we analyse the migration of an equilibrium droplet ‘in vitro’. That is, we characterize the migration of a single near-equilibrium droplet in an ambient flux field (see Figure 6). Our analysis is motivated by the findings of Glasner and Witelski [8, 9] for one-dimensional substrates. Our goal is to characterize how the ‘response’ of the droplet depends on its radius R . Our main effort is targeted towards a two-dimensional substrate. For comparison, we treat the much easier case of a one-dimensional substrate in Appendix D. It turns out that, at least in terms of scaling in R , the two-dimensional case does not differ from the one-dimensional case.

As we shall see, the scaling of the response in R depends on the exponent q in the mobility function (cf. (1.3)). The values of $q=3$ (not surprisingly) and $q=2$ (more surprisingly) play a special role. For $q < 2$, the variable mobility does not affect the propensity of the droplet to migrate. On the other hand, starting from $q > 3$, the effect of variable mobility saturates.

We give now a summary of this section. In Subsection 3.1, we introduce the set-up of a near-equilibrium droplet immersed into an ambient flux field. We implicitly characterize the migration velocity by the Rayleigh principle and by a solvability condition. In Subsection 3.2, we derive a semi-explicit formula for the migration velocity. It involves the solution of two auxiliary problems for pressures ψ_0 and ψ_1 . We also argue that the droplet always migrates opposite to the flux imposed far away. In Subsection 3.3, we state our results on the scaling of the migration speed in the droplet radius $R \gg 1$. The detailed analysis is presented in Appendices A and B, where we characterize the solutions ψ_1 and ψ_0 , respectively, of the two auxiliary problems introduced in Subsection 3.2. For ψ_1 , we use arguments which could be made rigorous in the framework of Γ -convergence. For ψ_0 , we use conventional asymptotic analysis.

In Appendix C, we compare the migration of a droplet in a flux field to the sliding of a droplet in an external potential. The latter situation was analysed by Pismen and Pomeau [15], but we obtain different results.

3.1 Set-up for migration

We want to characterize the migration speed of a near-equilibrium droplet immersed into an environment with prescribed constant flux J_∞ far away from the droplet. We let X denote the center of mass of the droplet and write

$$r = |x - X| \quad \text{and} \quad v = \frac{x - X}{r}.$$

We claim that the migration speed \dot{X} of the droplet, together with the flux field J , is characterized by the following problem:

$$-\dot{X} \cdot \nabla \bar{h} - \nabla \cdot (\bar{m} \nabla \mu) = 0, \quad (3.1)$$

$$J \cdot v \rightarrow J_\infty \cdot v \quad \text{as } r \uparrow \infty \quad \text{where} \quad J := -\bar{m} \nabla \mu, \quad (3.2)$$

$$\int \mu \nabla \bar{h} dx = 0. \quad (3.3)$$

We think of (3.1) as an elliptic equation for the pressure μ with the flux boundary conditions (3.2). Here and in the sequel, $\bar{m} := m(\bar{h})$ denotes the space-dependent mobility function for the equilibrium droplet shape \bar{h} .

We shall give two arguments in favor of (3.1), (3.2) and (3.3). The first is based on the Rayleigh principle (cf. Subsection 1.2), the second one on a solvability argument. By the Rayleigh principle, the flux J and the migration speed \dot{X} minimize *as a couple* the total dissipation rate D

$$\frac{1}{2} D = \frac{1}{2} \int \frac{1}{\bar{m}} |J|^2 dx, \quad (3.4)$$

subject to the continuity equation

$$-\dot{X} \cdot \nabla \bar{h} + \nabla \cdot J = 0 \quad (3.5)$$

with the boundary condition

$$J \cdot v \rightarrow J_\infty \cdot v \quad \text{as } r \uparrow \infty.$$

Hence the droplet migrates in order to minimize the overall dissipation rate under the flux boundary condition, which is a purely kinetic effect.

The variation in J yields that J is of the form

$$J = -\bar{m} \nabla \mu, \quad (3.6)$$

so that (3.5) turns into (3.1). Since (3.5) can be formulated as

$$\nabla \cdot (-\dot{X} (\bar{h} - \bar{h}_\infty) + J) = 0, \quad (3.7)$$

the variation of (3.4) w.r.t. \dot{X} yields (3.3):

$$0 = \int \frac{1}{\bar{m}} (\bar{h} - \bar{h}_\infty) J dx \stackrel{(3.6)}{=} - \int (\bar{h} - \bar{h}_\infty) \nabla \mu dx = \int \mu \nabla \bar{h} dx. \quad (3.8)$$

We now argue that (3.3) can also be interpreted in a more traditional way as solvability condition. We are interested in a solution of the thin-film equation, which we rewrite as

$$\partial_t h - \nabla \cdot (m(h) \nabla \mu) = 0, \quad (3.9)$$

$$\mu = -\Delta h + U'(h), \quad (3.10)$$

with the flux boundary conditions

$$J := -m(h) \nabla \mu \rightarrow J_\infty \quad \text{as } |x - X| \uparrow \infty.$$

We seek a solution of the form

$$h = \bar{h}(x - X(t)) + h_1(t, x), \quad (3.11)$$

where we think of h_1 as a perturbation of the equilibrium droplet profile \bar{h} . The latter is characterized by

$$-\Delta \bar{h} + U'(\bar{h}) = U'(\bar{h}_\infty), \quad (3.12)$$

(cf. Section 2). Notice that (3.12) implies (a consequence of translational invariance)

$$-\Delta \nabla \bar{h} + U''(\bar{h}) \nabla \bar{h} = 0. \quad (3.13)$$

In view of (3.12), up to the order of the perturbation (3.10) is

$$\mu = U'(\bar{h}_\infty) - \Delta h_1 + U''(\bar{h}) h_1. \quad (3.14)$$

Testing (3.14) with the exponentially decaying $\nabla \bar{h}$ yields (3.3):

$$\begin{aligned} \int \mu \nabla \bar{h} dx &\stackrel{(3.14)}{=} \int (-\Delta h_1 + U''(\bar{h}) h_1) \nabla \bar{h} dx \\ &= \int h_1 (-\Delta \nabla \bar{h} + U''(\bar{h}) \nabla \bar{h}) dx \stackrel{(3.13)}{=} 0. \end{aligned} \quad (3.15)$$

On the other hand, (3.11) inserted into (3.9) yields (3.1) to leading order. Indeed, we may replace $m(h)$ by its leading order $m(\bar{h}) = \bar{m}$ since $\mu = U'(\bar{h}_\infty) = \text{const}$ to leading order (cf. (3.14)). A broader analogy to systematic asymptotic expansions is described in Appendix F.

3.2 Characterization and sign of the migration velocity

The problem (3.1), (3.2) and (3.3) defines a linear relationship between the flux at infinity, J_∞ , and the droplet migration speed \dot{X} , which we want to characterize more explicitly.

We consider the 1- d substrate in Appendix D.1. For a 2- d substrate, we introduce two auxiliary problems: Let ψ_0 denote the solution of the homogeneous equation with

inhomogeneous boundary conditions, i.e.,

$$\begin{aligned} -\nabla \cdot (\bar{m} \nabla \psi_0) &= 0, \\ J_0 \cdot v &\rightarrow \begin{pmatrix} 1 \\ 0 \end{pmatrix} \cdot v \quad \text{as } |x| \uparrow \infty \quad \text{where } J_0 := \bar{m} \nabla \psi_0 \end{aligned} \quad (3.16)$$

(note the change of sign in the definition of J_0 , which is convenient for later purposes) and ψ_1 the solution of the inhomogeneous equation with homogeneous boundary conditions, i.e.

$$\begin{aligned} -\partial_1 \bar{h} - \nabla \cdot (\bar{m} \nabla \psi_1) &= 0, \\ J_1 \cdot v &\rightarrow 0 \quad \text{as } |x| \uparrow \infty \quad \text{where } J_1 := -\bar{m} \nabla \psi_1, \end{aligned} \quad (3.17)$$

Notice that both auxiliary problems allow for a physical interpretation: Problem (3.16) determines the pressure $-\psi_0$ which arises from a non-zero flux-boundary condition at infinity in a locally perturbed environment described by a variable mobility \bar{m} . Problem (3.17) determines the pressure ψ_1 which is necessary to make the equilibrium droplet migrate at unit speed. From (3.1) and (3.2) we read off that μ must be of the form

$$\mu = -J_\infty \psi_0 + \dot{X} \psi_1.$$

Here and in the sequel, we invoke isotropy to identify the vectors J_∞ and \dot{X} with the scalars in $\begin{pmatrix} J_\infty \\ 0 \end{pmatrix}$ and $\begin{pmatrix} \dot{X} \\ 0 \end{pmatrix}$, respectively. Hence (3.3) turns into

$$\dot{X} = \frac{\int \psi_0 \partial_1 \bar{h} dx}{\int \psi_1 \partial_1 \bar{h} dx} J_\infty. \quad (3.18)$$

Let us argue how the 2- d formula (3.18) relates to the 1- d formula (D 1). Substituting $\partial_1 \bar{h}$ in (3.18) according to (3.17) and *formally* integrating by parts yields

$$\dot{X} = \frac{\int \bar{m} \nabla \psi_0 \cdot \nabla \psi_1 dx}{\int \bar{m} \nabla \psi_1 \cdot \nabla \psi_1 dx} J_\infty = - \frac{\int \frac{1}{\bar{m}} J_0 \cdot J_1 dx}{\int \frac{1}{\bar{m}} |J_1|^2 dx} J_\infty. \quad (3.19)$$

On a 1- d substrate, (3.19) coincides with (D 1) since then, the solution of (3.16) is $J_0 \equiv 1$ and that of (3.17) is $J_1 = \bar{h} - \bar{h}_\infty$.

However, the integration by parts is allowed only in the denominator of (3.19). Indeed, since \bar{h} depends only on $r = |x - X|$, it is convenient to introduce polar coordinates

$$x - X = \begin{pmatrix} r \cos \varphi \\ r \sin \varphi \end{pmatrix}.$$

In this notation, both ψ_0 and ψ_1 are of the form

$$\psi_i(x) = \psi_i(r) \cos \varphi, \quad (3.20)$$

(it will always be clear from the context whether we mean $\psi_i(x)$ or $\psi_i(r)$) where the

functions $\psi_i(r)$ are determined by

$$\begin{aligned} -\partial_r(\bar{m}\partial_r\psi_0) - \frac{\bar{m}}{r}\partial_r\psi_0 + \frac{\bar{m}}{r^2}\psi_0 &= 0, \\ \psi_0(r=0) &= 0, \quad \lim_{r\uparrow\infty}\partial_r\psi_0 = 1, \end{aligned} \quad (3.21)$$

and

$$\begin{aligned} -\partial_r(\bar{h} - \bar{h}_\infty) - \partial_r(\bar{m}\partial_r\psi_1) - \frac{\bar{m}}{r}\partial_r\psi_1 + \frac{\bar{m}}{r^2}\psi_1 &= 0, \\ \psi_1(r=0) &= 0, \quad \lim_{r\uparrow\infty}\partial_r\psi_1 = 0, \end{aligned} \quad (3.22)$$

respectively. We also recall that up to exponentially small terms, the film height is constant in the precursor film:

$$\bar{h} = \bar{h}_\infty \quad \text{for } r - R \gg 1,$$

where R denotes the mesoscopic droplet radius (cf. Section 2). Hence in particular the coefficient \bar{m} is constant there:

$$\bar{m}_\infty = \text{const} \quad \text{for } r - R \gg 1.$$

Since $\{r, r^{-1}\}$ is a fundamental system of solutions of the constant coefficient ODE $-\partial^2 - r^{-1}\partial_r + r^{-2}$, we infer the following form of the solutions of (3.21) and (3.22) in the precursor film

$$\left. \begin{aligned} \psi_0 &= r + \frac{\text{const}}{r} \\ \psi_1 &= \frac{\text{const}}{r} \end{aligned} \right\} \quad \text{for } r - R \gg 1. \quad (3.23)$$

This asymptotic behaviour justifies the integration by parts of the denominator in (3.18):

$$\int \psi_1 \partial_1(\bar{h} - \bar{h}_\infty) dx = - \int \psi_1 \nabla \cdot (\bar{m} \nabla \psi_1) dx = \int \bar{m} |\nabla \psi_1|^2 dx,$$

but shows that the numerator in (3.18) has to be kept as is:

$$\dot{X} = \frac{\int \psi_0 \partial_1 \bar{h} dx}{\int \bar{m} |\nabla \psi_1|^2 dx} J_\infty, \quad (3.24)$$

or in polar coordinates

$$\dot{X} = \frac{\int_0^\infty \psi_0 \partial_r \bar{h} r dr}{\int_0^\infty \bar{m} ((\partial_r \psi_1)^2 + r^{-2} \psi_1^2) r dr} J_\infty.$$

The factor which relates \dot{X} to J_∞ has the same sign as for 1- d substrates:

$$\frac{\int_0^\infty \psi_0 \partial_r \bar{h} r dr}{\int_0^\infty \bar{m} ((\partial_r \psi_1)^2 + r^{-2} \psi_1^2) r dr} < 0.$$

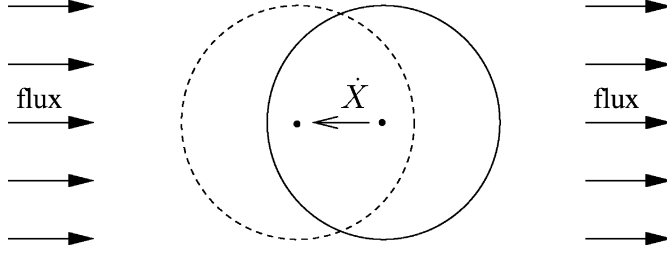


FIGURE 6. The droplet migrates in opposite direction to the ambient flux field J_∞ .

In particular, the droplet in the ambient flux field J_∞ migrates in opposite direction (see Figure 6).

Indeed, we have on the one hand

$$\partial_r \bar{h} \leq 0 \quad \text{for } r > 0,$$

and on the other hand

$$\psi_0 > 0 \quad \text{for all } r > 0. \quad (3.25)$$

The latter can be obtained as follows: Notice that (3.23) yields in particular that $\psi_0 \geq 0$ for sufficiently large r . Together with $\psi_0(r=0) = 0$ we infer from the maximum principle for $-\partial_r \bar{m} \partial_r - r^{-1} \bar{m} \partial_r + r^{-2} \bar{m}$ that

$$\psi_0 \geq 0 \quad \text{for all } r \geq 0. \quad (3.26)$$

By uniqueness for the second-order ODE (3.21), this improves to (3.25). Indeed, by (3.26), a point $r_0 > 0$ with $\psi_0(r_0) = 0$ would also satisfy $\partial_r \psi_0(r_0) = 0$ so that $\psi_0 \equiv 0$.

3.3 Scaling of migration velocity

We now address the scaling of the migration factor (3.24) in the droplet radius R for large radius $R \gg 1$. We treat the one-dimensional case (D 1) in Appendix D.1.1 following the analysis in [9, Appendix A].

In Appendices A and B we show that the migration factor on 2- d substrates has the *same scaling behaviour* in $R \gg 1$. More precisely, we show that

$$\int \bar{m} |\nabla \psi_1|^2 dx \approx \begin{cases} \frac{\pi}{12} R^4 & \text{for } q = 0, \\ C_q^1 R^{4-q} & \text{for } q \in (0, 3), \\ \frac{\pi}{\sqrt{2}} R \ln R & \text{for } q = 3, \\ C_q^1 R & \text{for } q > 3, \end{cases} \quad (3.27)$$

$$-\int \psi_0 \partial_1 \bar{h} dx \approx \begin{cases} \frac{\pi}{4\sqrt{2}} R^3 & \text{for } q = 0, \\ C_q^0 R^{3-q} & \text{for } q \in (0, 2), \\ \sqrt{2}\pi R \ln R & \text{for } q = 2, \\ C_q^0 R & \text{for } q > 2. \end{cases} \quad (3.28)$$

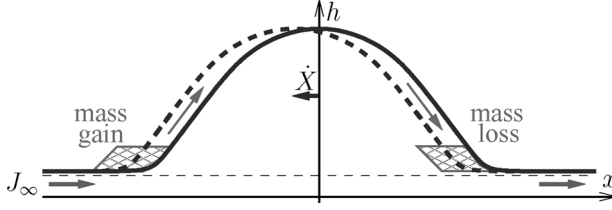


FIGURE 7. The response \dot{X} of the droplet on the flux J_∞ for mobility exponent $q < 2$. The deposited mass moves up the western flank.

As in the one-dimensional case (Appendix D.1.1), the main contribution to (3.27) for $0 < q < 3$ and to (3.28) for $0 < q < 2$ comes from the cap region, whereas it comes from the foot region for $q > 3$ and $q > 2$, respectively. In particular, the constants for $q > 3$ and $q > 2$, respectively, depend on the form of U . The most explicit expressions can be given at the cross-over values of q , at which the linear slope in the foot dominates. Let us also mention that when $U(h) = U_{\text{meso}}(h)$ (defined in (2.27)) for $q > 2$, $C_q^0 = \frac{\sqrt{2}\pi}{(q-2)(q-1)}$.

Thus we obtain for the migration factor (cf. (3.24))

$$-\frac{\dot{X}}{J_\infty} \approx \begin{cases} C R^{-1} & \text{for } q \in [0, 2), \\ C (\ln R) R^{-1} & \text{for } q = 2, \\ C R^{q-3} & \text{for } q \in (2, 3), \\ C \ln^{-1} R & \text{for } q = 3, \\ C & \text{for } q > 3. \end{cases} \quad (3.29)$$

Hence larger droplets migrate slower. However, the stronger the monotonicity of $m(h)$ as parameterized by the exponent q , the less pronounced is this effect; for $q > 3$, there is no R -dependence to leading order. There are two cross-overs at $q = 2$ and $q = 3$: Up to $q = 2$, the scaling of the response is independent of q , and starting from $q = 3$, the scaling exponent saturates.

The scaling R^{-1} of the migration factor (3.29), which holds for $q < 2$, is easy to interpret: Consider a droplet moving under the effects of a prescribed flux at infinity. For clarity, let us say that the prescribed flux has the eastwards direction. In a small time interval δt , the amount of mass deposited at the western foot region (which has size $\sim R^{d-1}$) scales as $\delta t |J_\infty| R^{d-1}$; the same amount is taken away from the eastern side. By this, the center of mass X of the droplet moves westwards by $\delta X \sim \delta t |J_\infty| R^{-1}$, so that it is natural that the new center of the equilibrium droplet moves westwards by the same amount. One can visualize this by thinking that the mass deposited at the western foot moves up the droplet flank (see Figure 7). At the eastern flank, the same amount of mass moves down to compensate the mass loss at the foot.

When $q > 2$, as mobility of droplets increases, the picture is not as simple. In a sense the disturbance to droplet shape caused by depositing mass at the western foot region is alleviated by the westward motion of the entire droplet. When $q > 3$, it is as if the mass deposited at the western foot does not move up the flank, but that the droplet cap instead slides westwards to cover the deposited mass (see Figure 8).

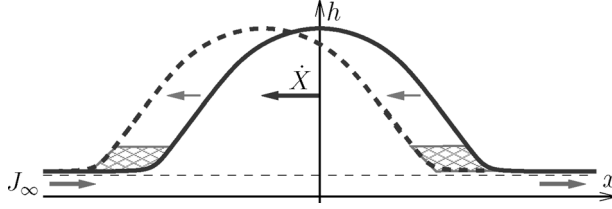


FIGURE 8. The response \dot{X} on the flux J_∞ for mobility exponent $q > 3$. The droplet cap slides on the mass deposited at the western foot.

Let us finally remark that the quantity in (3.28) and the asymptotic behaviour of ψ_1 are related: We claim that

$$\lim_{r \rightarrow \infty} r\psi_1(r) = \frac{1}{2\pi} \int_{\mathbb{R}^2} \psi_0 \partial_1 \bar{h} dx. \quad (3.30)$$

To show that consider $r \gg L$. Integrating by parts twice yields

$$\begin{aligned} & \int_{B(0,r)} \nabla \cdot (\bar{m} \nabla \psi_1) \psi_0 dx - \int_{B(0,r)} \psi_1 \nabla \cdot (\bar{m} \nabla \psi_0) dx \\ &= \int_{\partial B(0,r)} \bar{m} \psi_0 \nabla \psi_1 \cdot \frac{x}{|x|} dx - \int_{\partial B(0,r)} \bar{m} \psi_1 \nabla \psi_0 \cdot \frac{x}{|x|} dx. \end{aligned}$$

Using (3.16) and (3.17) we obtain

$$- \int_{B(0,r)} \partial_1 \bar{h} \psi_0 dx = \int_0^{2\pi} \psi_0(r) \partial_r \psi_1(r) \cos^2 \theta r d\theta - \int_0^{2\pi} \psi_1(r) \partial_r \psi_0(r) \cos^2 \theta r d\theta.$$

Using the asymptotic behaviour of $\psi_0(r)$ and ψ_1 obtained in (3.23)

$$\psi_0(r) \approx r, \quad \partial_r \psi_0(r) \approx 1, \quad \partial_r \psi_1(r) \approx -\frac{1}{r} \psi_1(r) \quad \text{as } r \rightarrow \infty.$$

by taking the limit $r \rightarrow \infty$ we obtain

$$- \int_{\mathbb{R}^2} \psi_0 \partial_1 \bar{h} dx = -2\pi \lim_{r \rightarrow \infty} r\psi_1(r). \quad (3.31)$$

4 Interacting mesoscopic droplets

While in the previous section we considered how a single droplet interacts with an ambient flux field, here we are interested in how droplets interact with each other. In particular we are interested in the regime of large, quasi-stationary, well-separated droplets. That is,

$$1 \ll R \sim V^{\frac{1}{d+1}} \ll L, \quad (4.1)$$

where R is the typical radius, V the typical volume of a droplet and L is the typical distance between droplets (defined as (number density of droplets) $^{-1/d}$).

We impose the quasi-stationarity of the system by reducing the configuration space to collections of stationary droplets. The stationary droplets have slightly different heights in the tail region; the discrepancy is comparable to $1/R$. In the case that the excess mass in the precursor is small compared to the droplet mass, that is when $R^2 \gg L$, the variation of the height in the precursor layer does not have an effect on the leading order dynamics. In our set-up one could deal with discrepancies in the tail region by smoothly replacing the tails by constant height 1 beyond some intermediate distance, \bar{d} , ($R \ll \bar{d} \ll L$).

However, we choose to deal with the tails by introducing a further reduction. That is, we study the system on the mesoscopic level. We reduce the configuration space to the mesoscopic shape of the droplets (2.23), that is to parabolic droplets of fixed contact angle on the precursor layer. Hence the configuration is fully described by the centers and volumes of the droplets.

The dynamics of the interacting droplets is determined by the Rayleigh principle, described in Subsection 1.2. That is, at any time the flux J (subject to the continuity equation) minimizes

$$\frac{1}{2}D + \dot{E}.$$

On the reduced configuration space we consider the mesoscopic energy (2.26)

$$E(h) = E_{\text{meso}}(h) = \int \frac{1}{2}|\nabla h|^2 + U_{\text{meso}}(h) dx, \quad (4.2)$$

for which the parabolic droplets are exact steady states (see (2.25)). We choose this reduction as it enables us to make the presentation simple and transparent.

The analysis of the previous section and that of ψ_0 and ψ_1 in Appendices A and B shows that for $q \leq 2$ the interaction of large droplets with their environment depends to leading order only on the mesoscopic profile, and not on the details of the potential U . In particular, the asymptotic values of the quantities in (3.27) and (3.28) rely only on the mesoscopic shape of the droplet. For $q > 2$ the dependence on the particular form of U is only through a U -dependent constant factor. Thus even though our reduced system neglects the precise shape of the droplet, the reduced dynamics differs from the actual limiting dynamics in the case of $q > 2$ only by a constant factor in the migration terms (see (4.25) and (4.26)).

We present the analysis only for the 2- d systems in detail. The analysis is not fully rigorous as it depends on conclusions of asymptotic analysis of Appendices A and B. We do however validate the smallness of the lower order terms in the approximations we carry out. Results of the 1- d analysis are given in Appendix D. They are in agreement with the conclusions of Glasner and Witelski [8, 9], who already studied the 1- d case with (different) asymptotic tools.

4.1 Reduced structure

In the following, we will introduce the reduced configuration space and the dynamical structure for both one and two dimensions.

Configuration space

The parabolic droplets, which are steady states of the mesoscopic energy (4.2), are parameterized by their volume V (above the precursor height) and center of mass X :

$$h_{V,X}(x) := \max \left\{ 0, -\frac{1}{\sqrt{2}\omega} V^{-\frac{1}{d+1}} |x - X|^2 + \frac{1}{\sqrt{2}} \omega V^{\frac{1}{d+1}} \right\}, \quad (4.3)$$

where

$$\omega := \begin{cases} \left(\frac{3}{2\sqrt{2}} \right)^{\frac{1}{2}} & \text{for } d = 1, \\ \sqrt{2}\pi^{-\frac{1}{3}} & \text{for } d = 2. \end{cases}$$

The constant ω is chosen such that the radius R and the volume V are related by

$$R = \omega V^{\frac{1}{d+1}}.$$

A configuration of n droplets is fully described by the position vector $(X_1^T, \dots, X_n^T)^T$ with $X_i \in \mathbb{R}^d$ and the volume vector $(V_1, \dots, V_n)^T$. We define

$$h_i(x) := h_{V_i, X_i}(x),$$

$$h_\Theta(x) := 1 + \sum_{i=1}^n h_i(x), \quad \Theta := (V_1, \dots, V_n, X_1^T, \dots, X_n^T)^T$$

and the droplet distances $L_{ij} := |X_i - X_j|$.

An infinitesimal change of a configuration Θ is described by the infinitesimal change of the droplet volumes and their centers, denoted by $\dot{\Theta}$:

$$\dot{\Theta} := (\dot{V}_1, \dots, \dot{V}_n, \dot{X}_1^T, \dots, \dot{X}_n^T)^T \in \mathbb{R}^{(d+1)n}.$$

Due to the conservation of mass the change vector $\dot{\Theta}$ is admissible, if $\sum_{i=1}^n \dot{V}_i = 0$, or in other words, if $\dot{\Theta}$ is orthogonal to

$$p = \frac{1}{\sqrt{n}}(1_n, 0_{dn})^T.$$

(Here we use the notation $z_k := (z, \dots, z) \in \mathbb{R}^k$, for $z \in \{0, 1\}$.) The infinitesimal change of the height profile h_Θ of the configuration corresponding to the change vector $\dot{\Theta}$ is given by

$$\Delta h_\Theta := \left. \frac{d}{ds} \right|_{s=0} h_{\Theta+s\dot{\Theta}} = \sum_{i=1}^n \frac{\partial h_i}{\partial V_i} \dot{V}_i - \nabla h_i \cdot \dot{X}_i,$$

where

$$\frac{\partial h_i}{\partial V_i} := \left. \frac{\partial h_{V_i, X_i}}{\partial V} \right|_{V=V_i} = \frac{1}{\sqrt{2}(d+1)\omega} V_i^{-\frac{d+2}{d+1}} |x - X_i|^2 + \frac{1}{\sqrt{2}(d+1)} \omega V_i^{-\frac{d}{d+1}} \quad (4.4)$$

for $x \in B(X_i, R_i)$.

Energy

On the restricted configuration space the energy has a simple form:

$$E(h_\Theta) = \frac{\sqrt{2}(d+1)}{\omega} \sum_{i=1}^n V_i^{\frac{d}{d+1}}. \quad (4.5)$$

Note that we skip the subscript ‘meso’ for convenience. The infinitesimal change of energy generated by the infinitesimal change of the configuration in the direction of $\dot{\Theta}$ is

$$\dot{E}[\dot{\Theta}] = \nabla E \cdot \dot{\Theta} = \frac{\sqrt{2}d}{\omega} \sum_{i=1}^n V_i^{-\frac{1}{d+1}} \dot{V}_i.$$

4.1.1 Reduced Rayleigh dynamics

Analogous to the simpler model problem in the previous section (see equations (3.4) and (3.5)), the trajectory $\Theta(t)$ of the system is determined by the fact that the change vector $\dot{\Theta}$ along with the flux J minimize as a pair the quantity

$$\frac{1}{2}D + \nabla E \cdot \dot{\Theta}$$

subject to

$$\Delta h_\Theta + \nabla \cdot J = 0.$$

The viscous dissipation rate is, as before, quadratic in J : $D = \int \frac{1}{m} |J|^2 dx$.

We already know that the minimizing flux is a gradient of a pressure, that is

$$J = -m\nabla\varphi_\Theta,$$

subject to

$$\Delta h_\Theta - \nabla \cdot (m\nabla\varphi_\Theta) = 0.$$

Consequently to determine $\dot{\Theta}$ one needs to minimize

$$\frac{1}{2} \int m |\nabla\varphi_\Theta|^2 dx + \nabla E \cdot \dot{\Theta}. \quad (4.6)$$

Approximately (at least in the sense, that the associated quadratic form of minimal dissipation, i.e. $D = \int m |\nabla\varphi_\Theta|^2 dx$, is well approximated in terms of the following model pressures as we will see later), the pressure φ_Θ is a linear combination of the following ‘decoupled’ ones:

- *Pressure relevant to droplet motion:* We recall the two auxiliary problems (3.16) and (3.17) in a slightly modified form. We introduce the pressures $\Psi_{0,V}$ (generated by a non-zero flux-boundary condition far from droplet) by

$$\begin{aligned} -\nabla \cdot (m\nabla\Psi_{0,V}) &= 0, \\ J_{0,V} \cdot v &\rightarrow \left(\frac{1}{0}\right) \cdot v \text{ as } |x| \uparrow \infty, \quad \text{where } J_{0,V} := m\nabla\Psi_{0,V}, \end{aligned} \quad (4.7)$$

and $\Psi_{1,V}$, which makes the droplet move with unit speed, by

$$\begin{aligned} -\partial_1 h_{V,0} - \nabla \cdot (m \nabla \Psi_{1,V}) &= 0, \\ J_{1,V} \cdot v &\rightarrow 0 \text{ as } |x| \uparrow \infty, \quad \text{where } J_{1,V} := -m \nabla \Psi_{1,V}. \end{aligned} \quad (4.8)$$

As before, $m = m(1 + h_{V,0})$. The subscript V highlights the dependence of m and h on the volume. Note that both $\Psi_{0,V}$ and $\Psi_{1,V}$ are centered in the origin in contrast to the pressures determined by (3.16) and (3.17). Furthermore, we use explicitly the mesoscopic droplet profile for the characterization.

Using the isotropy of the mobility in (4.8) we can determine the pressure corresponding to arbitrary droplet velocity vector $\dot{X} \in \mathbb{R}^2$ instead of $(1,0)^T$. We denote this pressure by $\Psi_{1,V}^{\dot{X}}$. It has a dipolar form:

$$\Psi_{1,V}^{\dot{X}}(x) = \Psi_{1,V}(|x|) |\dot{X}| \cos \theta \quad (4.9)$$

in the polar coordinates determined by

$$\frac{x}{|x|} \cdot \frac{\dot{X}}{|\dot{X}|} = \cos \theta.$$

- *Pressure relevant to droplet mass change:* We introduce the pressure needed to move the mass from a single mesoscopic droplet into the surrounding precursor film: Ψ_V is a radially symmetric solution of

$$\nabla \cdot (m \nabla \Psi_V) = -\frac{\partial h_{V,0}}{\partial V}. \quad (4.10)$$

Note that outside of the droplet Ψ_V satisfies the Laplace equation. For $r > R$, where $R = \omega V^{1/3}$ is the radius of the droplet, we have

$$1 = \int_{B(0,r)} \frac{\partial h_{V,0}}{\partial V} dx = - \int_{\partial B(0,r)} m \nabla \Psi_V \cdot v = -2\pi r (\partial_r \Psi_V).$$

Therefore we can determine the pressure outside of the droplet up to an additive constant

$$\Psi_V(x) = -\frac{1}{2\pi} \ln |x| + \text{const.} \quad \text{for } |x| > R. \quad (4.11)$$

Since $\varphi_{\dot{\theta}}$ depends linearly on the change $\dot{\theta}$, the first term in (4.6) defines a quadratic form in $\dot{\theta}$. The associated bilinear form is

$$D(\dot{\theta}, \dot{\xi}) := \int \frac{1}{m} J_{\dot{\theta}} \cdot J_{\dot{\xi}} dx = \int m \nabla \varphi_{\dot{\theta}} \cdot \nabla \varphi_{\dot{\xi}} dx \quad (4.12)$$

for admissible change vectors $\dot{\theta}$ and $\dot{\xi}$. Since the space of admissible change vectors is finite-dimensional, there is a symmetric matrix G representing the bi-linear form:

$$\dot{\theta}^T G \dot{\xi} = D(\dot{\theta}, \dot{\xi}).$$

Such matrix G is not unique. The canonical choice is the matrix \bar{G} which also satisfies $\bar{G}p = 0$. A symmetric matrix G represents the same bi-linear form on the set of admissible change vectors if and only if $\Pi G \Pi = \bar{G}$, where $\Pi = I - pp^T$ is the orthogonal projection to the orthogonal complement of p .

Minimizing (4.6) in the form $\dot{\Theta}^T G \dot{\Theta} + \nabla E \cdot \dot{\Theta}$ in $\dot{\Theta}$ with the constraint $\dot{\Theta} \cdot p = 0$ gives that $\dot{\Theta}$ is uniquely determined by

$$\begin{aligned} \Pi(G\dot{\Theta} + \nabla E) &= 0 \\ \dot{\Theta} \cdot p &= 0. \end{aligned} \quad (4.13)$$

In the following subsections, we will give asymptotic expressions for the entries of G in terms of the auxiliary pressures Ψ_V and $\Psi_{i,V}$ and solve the problem explicitly for a two-droplet configuration.

4.2 Coefficients of G in the two-dimensional case

As indicated previously, the coefficients of G describe the dissipation generated by the fluxes that correspond to volume changes and motion of droplets. For clarity, we subdivide the matrix $G \in \mathbb{R}^{3n \times 3n}$ into three sub-matrices: the volume change matrix $G^v \in \mathbb{R}^{n \times n}$, the migration matrix $G^m \in \mathbb{R}^{2n \times 2n}$ and the coupling matrix $C \in \mathbb{R}^{2n \times n}$:

$$G = \begin{bmatrix} G^v & C^T \\ C & G^m \end{bmatrix}. \quad (4.14)$$

4.2.1 Approximate coefficients of G

We show in Subsection 4.3 that

$$G_{ij}^v = \begin{cases} -\frac{1}{2} \left(\int_{B(0,L)} m |\nabla \Psi_{V_i}|^2 + \int_{B(0,L)} m |\nabla \Psi_{V_j}|^2 \right) + O(1) & \text{if } i \neq j, \\ 0 & \text{if } i = j, \end{cases} \quad (4.15)$$

$$G_{ij}^m = \begin{cases} \text{diag}(g_i, g_i) + o(g_i)_{2 \times 2} & \text{if } i = j, \\ o(\sqrt{g_i g_j})_{2 \times 2} & \text{else,} \end{cases} \quad (4.16)$$

where $o(f)_{2 \times 2} = \begin{bmatrix} o(f) & o(f) \\ o(f) & o(f) \end{bmatrix}$ and

$$g_i = \int m_i(x) |\nabla \Psi_{1,V_i}(x)|^2 dx, \quad (4.17)$$

where $m_i(x) := m(1 + h_i(x + X_i))$ and Ψ_{1,V_i} is defined in (4.8). The coupling coefficients are given by

$$C_{ij} \begin{cases} = \frac{X_i - X_j}{|X_i - X_j|} c_{ij} + o(c_{ij})_{2 \times 1} & \text{if } i \neq j, \\ 0 & \text{else,} \end{cases} \quad (4.18)$$

where, using (3.31),

$$c_{ij} = \frac{1}{2\pi} \frac{1}{|X_i - X_j|} \int \partial_1 h_i(x + X_i) \Psi_{0, V_i}(x) dx = \frac{1}{|X_i - X_j|} \lim_{r \rightarrow \infty} r \Psi_{1, V_i}(r) \quad (4.19)$$

and Ψ_{0, V_i} is defined in (4.7).

Asymptotic values of relevant quantities

Let $L_{ij} = |X_i - X_j|$. We consider the regime $\min_{i \neq j} L_{ij} \gg \max_i R_i$. We furthermore require that droplets are of comparable sizes in that $\frac{L_{ij}}{R_i} \gg \left(\frac{R_i}{R_j}\right)^3$ for all i, j . In Subsection 4.3 we show that for $i \neq j$

$$G_{ij}^v = -\frac{1}{4\pi} (\ln(L_{ij}/V_i^{\frac{1}{3}}) + \ln(L_{ij}/V_j^{\frac{1}{3}})) + O(1).$$

The asymptotic values of g_i and c_{ij} for $i, j = 1, 2$ and $i \neq j$ follow from (3.27) and (3.28):

$$g_i = \begin{cases} C V_i^{\frac{4-q}{3}} & \text{for } q \in [0, 3), \\ \frac{\pi^{\frac{2}{3}}}{3} V_i^{\frac{1}{3}} \ln V_i & \text{for } q = 3, \\ C V_i^{\frac{1}{3}} & \text{for } q > 3, \end{cases} \quad (4.20)$$

$$c_{ij} = -\frac{1}{L_{ij}} \begin{cases} C V_i^{\frac{3-q}{3}} & \text{for } q \in [0, 2), \\ \frac{1}{3\pi^{\frac{4}{3}}} V_i^{\frac{1}{3}} \ln V_i & \text{for } q = 2, \\ C V_i^{\frac{1}{3}} & \text{for } q > 2. \end{cases} \quad (4.21)$$

Rayleigh dynamics of two droplets

As an insightful illustration we consider the particular case of two droplets in detail. Let us compute the equations for $\hat{\Theta}$ in the natural coordinates for the two-droplet configuration $[e_1, e_2]$:

$$e_1 = \frac{X_2 - X_1}{|X_2 - X_1|}, \quad e_2 \perp e_1, \quad |e_2| = 1 \quad (4.22)$$

The characterization of G given in (4.15)–(4.19) yields

$$G = \begin{bmatrix} 0 & G_{12}^v & 0 & 0 & c_{21} & 0 \\ G_{12}^v & 0 & -c_{12} & 0 & 0 & 0 \\ 0 & -c_{12} & g_1 & 0 & 0 & 0 \\ 0 & 0 & 0 & g_1 & 0 & 0 \\ c_{21} & 0 & 0 & 0 & g_2 & 0 \\ 0 & 0 & 0 & 0 & 0 & g_2 \end{bmatrix}.$$

We obtain that the dynamics according to (4.13) is given by the following system of ODEs:

$$\begin{aligned}
\dot{V}_1 + \dot{V}_2 &= 0, \\
-G_{12}^v \dot{V}_1 + G_{21}^v \dot{V}_2 + c_{12} \dot{X}_1^1 + c_{21} \dot{X}_2^1 &= -\frac{2\sqrt{2}}{\omega} (V_1^{-\frac{1}{3}} - V_2^{-\frac{1}{3}}), \\
g_1 \dot{X}_1^1 - c_{12} \dot{V}_2 &= 0, \\
\dot{X}_1^2 &= 0, \\
g_2 \dot{X}_2^1 + c_{21} \dot{V}_1 &= 0, \\
\dot{X}_2^2 &= 0.
\end{aligned}$$

Solving the system yields in particular

$$\dot{V}_1 = \frac{2\sqrt{2}}{\omega} \left(2G_{12}^v + \frac{c_{12}^2}{g_1} + \frac{c_{21}^2}{g_2} \right)^{-1} (V_1^{-\frac{1}{3}} - V_2^{-\frac{1}{3}}). \quad (4.23)$$

Using (4.20) and (4.21), the assumption $L_{12} \gg V_i^{\frac{1}{3}}$ for $i = 1, 2$ yields

$$-G_{12}^v \gg 1 \gg \frac{c_{12}^2}{g_i}. \quad (4.24)$$

Therefore the system of ODEs in the limit reduces to

$$\dot{V}_1 = -\frac{4\pi^{\frac{4}{3}}}{\ln(L/V_1^{\frac{1}{3}}) + \ln(L/V_2^{\frac{1}{3}})} (V_1^{-\frac{1}{3}} - V_2^{-\frac{1}{3}}), \quad (4.25)$$

$$\dot{X}_1^1 = -\frac{c_{12}}{g_1} \dot{V}_1, \quad \dot{X}_2^1 = -\frac{c_{21}}{g_2} \dot{V}_1. \quad (4.26)$$

Hence, both droplets move in the direction of the smaller one, whose volume decreases. Figure E 2 in Appendix E shows the migration in a two-droplet configuration. In particular, it reveals the q -dependence of the droplet velocity in accordance with the leading order scaling of the migration factor.

The equations (4.26) for the motion of the droplets provide a nice way of interpreting the connection between J_∞ in the model problem in Section 3 and the case of a configuration of droplets with at least two droplets. For this purpose, consider the equation of motion (4.13) that is

$$\begin{aligned}
\dot{X}_1 &= -\frac{\dot{V}_2}{g_1} C_{12} = \frac{\int \partial_1 h_1 \Psi_{0,V_1}(x - X_1) dx}{\int m_1 |\nabla \Psi_{1,V_1}(x - X_1)|^2 dx} \left(-\frac{\dot{V}_2}{2\pi} \frac{X_1 - X_2}{|X_1 - X_2|^2} \right) \\
&= \frac{\int \partial_1 h_1 \Psi_{0,V_1}(x - X_1) dx}{\int m_1 |\nabla \Psi_{1,V_1}(x - X_1)|^2 dx} \left(-\nabla \left(\frac{\dot{V}_2}{2\pi} \ln |X_1 - X_2| \right) \right),
\end{aligned}$$

and compare it to (3.24) in Section 3. It reveals that in the context of a two-droplet system, J_∞ can be interpreted as the flux at X_1 generated by the harmonic potential which transports mass \dot{V}_2 out of the droplet centered in X_2 .

4.2.2 Time scales of the dynamics

To deduce heuristically the typical time scale of Ostwald ripening and migration from the reduced structure we assume that the typical length scales (like the typical droplet radius) exhibit scaling in time. In addition to scaling in V , we consider how the scaling depends on the average film height \bar{H} , up to logarithmic corrections. Note that the mass conservation dictates that

$$\bar{H}L^d = V. \quad (4.27)$$

Heuristically, these time scales allow us to identify the dominant coarsening mechanism in different regimes.

The equation (4.25) describes the mass transfer rate between two droplets. It follows

$$\dot{V} \sim \frac{1}{\ln V} V^{-\frac{1}{3}},$$

where we use (4.27). Hence the time scale for ripening is

$$\tau_{\text{rip}} = \frac{V}{\dot{V}} = V^{\frac{4}{3}} \ln V. \quad (4.28)$$

We expect that $\dot{L} \sim |\dot{X}|$ and thus

$$\dot{L} \sim |\dot{X}_i| \sim \frac{1}{\ln L} V^{-\frac{1}{3}} \frac{1}{L} \begin{cases} V^{-\frac{1}{3}} & \text{for } q \in [0, 2), \\ V^{-\frac{1}{3}} \ln V & \text{for } q = 2, \\ V^{\frac{q-3}{3}} & \text{for } q \in (2, 3), \\ \frac{1}{\ln V} & \text{for } q = 3, \\ 1 & \text{for } q > 3. \end{cases} \quad (4.29)$$

Therefore the time scale for migration of droplets is

$$\tau_{\text{mig}} = \frac{L}{\dot{L}} \sim \frac{1}{\bar{H}} V^{\frac{4}{3}} \ln V \begin{cases} V^{\frac{1}{3}} & \text{for } q \in [0, 2), \\ \frac{V^{\frac{1}{3}}}{\ln V} & \text{for } q = 2, \\ V^{\frac{3-q}{3}} & \text{for } q \in (2, 3), \\ \ln V & \text{for } q = 3, \\ 1 & \text{for } q > 3. \end{cases} \quad (4.30)$$

Note that $\tau_{\text{mig}} \gg \tau_{\text{rip}}$ if $q < 3$ and $V \gg 1$ which indicates that droplets are nearly stationary. When $q = 3$ the difference between time scales is only logarithmic in V , while when $q > 3$ they are comparable. It is also worth noting the scaling in the average film height: The importance of motion of droplets grows if the average film thickness is increased.

In the two-dimensional case, the fact that a droplet migrates over a distance L does not necessarily imply collision with another droplet, since droplets might miss each other. In

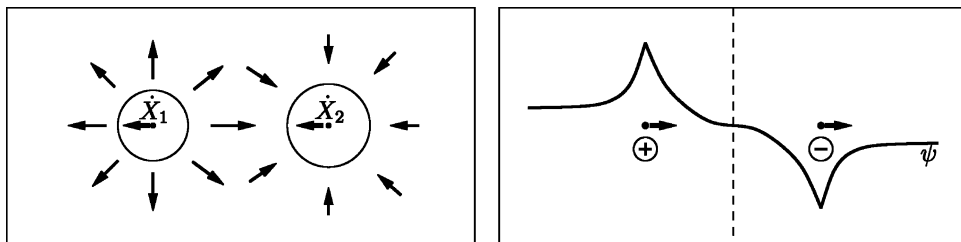


FIGURE 9. Left: Two isolated droplets of different size generate a flux field J , which transports mass from the smaller droplet to the larger one. Right: The flux J is the gradient of a harmonic function ψ . For both droplets, the constant part of $-\nabla\psi$ in an annular region of the droplet (playing the role of J_∞) points eastwards, and therefore gives rise to migration to the west.

the following, we will give formal arguments that on the one hand, a configuration of two isolated droplets cannot lead to collision, whereas on the other hand, a configuration of two relatively small droplets submerged into a matrix of larger droplets generically leads to collision.

A configuration of two isolated droplets will not lead to collision: Consider two droplets with volumes $V_1 < V_2$ and centers of mass X_1 and X_2 , respectively (see Figure 9 (left)). As we found out earlier, mass exchange between droplets gives rise to a flux field J . In the precursor, J is the gradient of a harmonic function: $J = -\nabla\psi$, where ψ has the form of a harmonic function $\frac{1}{2\pi}(\dot{V}_1 \ln(x-X_1) + \dot{V}_2 \ln(x-X_2))$ (see Figure 9 (right) for a cross section). In an annular region around a given droplet centered at X , it makes sense to speak of the linear part of ψ (in the sense of a Laurent expansion). This linear part, or more precisely, its constant gradient, plays the role of the flux J_∞ as we pointed out in the previous subsection. Hence, it is this linear part which determines the migration speed \dot{X} of the droplet.

Here, the constant part of $-\nabla\psi$ in an annular region around a droplet is parallel to $X_2 - X_1$ due to the symmetry of the problem. Furthermore, it holds for both droplets that this constant part has positive slope in the direction of $X_2 - X_1$. Since $\dot{V}_1 = -\dot{V}_2$, it even holds that the constant parts are equal. Thus, according to the considerations above, both droplets move westwards in the direction of the smaller droplet. As the scaling of the migration factor (3.29) reveals, the smaller droplet moves faster than the larger one. Therefore, collision cannot happen in a two-droplet configuration. By this, we obtain a different result than Pismen and Pomeau in [15] in the following sense: They claim that both droplets migrate in the direction of the larger droplet, that is eastwards in our picture. Furthermore, they argue (in accordance with our findings) that the smaller droplet moves faster, so that it might catch up with the larger one leading to collision. In contrast, numerical tests confirm our findings (see Figure E 2 in Appendix E).

However, in many-droplet configurations, there is a bias towards collision of small droplets: Consider two relatively small droplets submerged into a configuration of larger droplets. We find that both droplets lose mass to the surrounding droplets (see Figure 10 (left)). Furthermore, the specific form of ψ (see Figure 10 (right)) yields constant parts of $-\nabla\psi$, which on the one hand points westwards in the neighbourhood of the western droplet, and on the other hand points eastwards in the neighbourhood of the eastern droplet. Here, we again invoke the symmetry of the problem. Accordingly, the droplets move towards each other, which eventually leads to collision, provided no droplet vanishes.

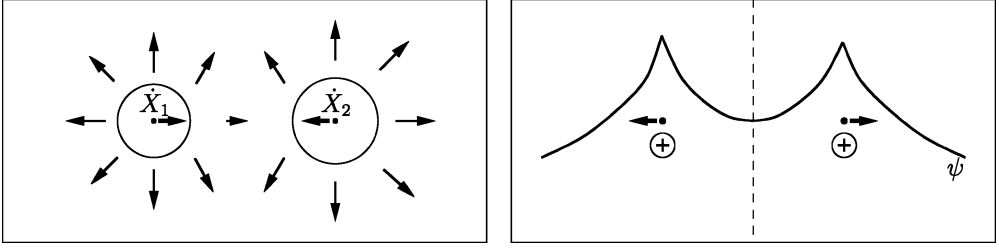


FIGURE 10. Left: Two smaller droplets submerged into a configuration of larger droplets. They both lose mass to the surrounding droplets. Right: The constant part of $-\nabla\psi$ points westwards in the neighbourhood of the western droplet, and eastwards in the neighbourhood of the eastern droplet. Therefore, the droplets move towards each other.

Hence for $q \geq 3$, the average film height \bar{H} sets the relative importance of collision for the coarsening process for all times (up to a logarithm for $q = 3$). In particular, we expect a collision-dominated coarsening scenario for configurations with large average height.

4.3 Derivation of the coefficients of G

We present the details of the derivation of coefficients of G only for a configuration of two droplets. It contains all the essential ingredients of the derivation with n droplets present, but is significantly easier to present. Accordingly, we consider a configuration of two droplets, $\Theta = (V_1, V_2, X_1^T, X_2^T)^T$. Let $L = |X_2 - X_1|$.

4.3.1 Computing G^v

Consider the general mass exchange given by the change vector $v = (\dot{V}_1, \dot{V}_2, 0_4)^T$ with $\dot{V}_1 + \dot{V}_2 = 0$. Then

$$\Delta h_v(x) = \frac{\partial h_1}{\partial V_1}(x) \dot{V}_1 + \frac{\partial h_2}{\partial V_2}(x) \dot{V}_2. \quad (4.31)$$

By the definition of the dissipation rate (4.12) it follows that

$$G_{11}^v (\dot{V}_1)^2 + G_{22}^v (\dot{V}_2)^2 + 2G_{12}^v \dot{V}_1 \dot{V}_2 = v^T G v = \int_{\mathbb{R}^2} m |\nabla \varphi_v(x)|^2 dx,$$

where

$$\nabla \cdot (m \nabla \varphi_v) = \Delta h_v. \quad (4.32)$$

The above condition fully determines the volume exchange part of the bi-linear form, D , but, as we discussed before, the matrix G is not unique. Since we have in mind the dissipation due to mass exchange it is natural to choose G for which $G_{11}^v = G_{22}^v = 0$, which implies

$$2G_{12}^v \dot{V}_1 \dot{V}_2 = \int_{\mathbb{R}^2} m |\nabla \varphi_v(x)|^2 dx.$$

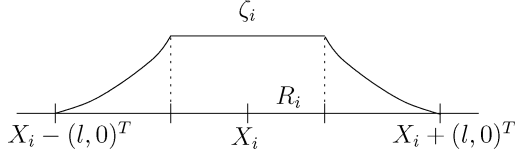


FIGURE 11. The test function ζ_i carries the mass \dot{V}_i outside the i -th droplet.

To determine the value on the right hand side, we will show that φ_v is, in a sense, well approximated by $-\dot{V}_1 \Psi_{V_1}(\cdot - X_1) - \dot{V}_2 \Psi_{V_2}(\cdot - X_2)$. We start by observing that an elementary computation based on (4.11) shows that for $i = 1, 2$

$$\int_{B(0,L) \setminus B(0,R_i)} m |\nabla \Psi_{V_i}|^2 dx = \frac{1}{2\pi} \ln(L/V_i^{1/3}) + O(1). \quad (4.33)$$

Let us now show that the integral over $B(0, R_i)$ is of size $O(1)$. Consider $J_i(x) := -m(x) \nabla \Psi_{V_i}(x)$. Then $\nabla \cdot J_i = \frac{\partial h}{\partial V}|_{V=V_i}$. Let $y = x/R_i$. Let $\tilde{J}(y)$ be the radially symmetric solution of $\nabla_y \cdot \tilde{J}(y) = \frac{\partial h}{\partial V}|_{V=1}$. The scaling property of the family of steady states yields that $\tilde{J}(y) = R_i J_i(x)$. Therefore

$$\int_{B(0,R_i)} m |\nabla \Psi_{V_i}|^2 \leq \int_{B(0,R_i)} |J_i(x)|^2 dx = \int_{B(0,1)} |\tilde{J}(y)|^2 dy, \quad (4.34)$$

which proves the claim.

Thus we need to show that $-2G_{12}^v = \frac{1}{2\pi}(\ln(L/V_1^{1/3}) + \ln(L/V_2^{1/3})) + O(1)$. Note that there are two representations of $\int m |\nabla \varphi_v(x)|^2 dx$:

$$\int m |\nabla \varphi_v(x)|^2 dx = \max_{\zeta} \left\{ \int -m |\nabla \zeta(x)|^2 + 2\Delta h_v(x) \zeta(x) dx \right\} \quad (4.35)$$

$$= \min_J \left\{ \int \frac{1}{m} |J|^2 dx \mid \nabla \cdot J = \Delta h_v \right\}. \quad (4.36)$$

In the following, we provide lower and upper bounds on $\int m |\nabla \varphi_v(x)|^2 dx$ that differ by an amount of $O(1)$.

Lower bound. Let $l = L/3$. To construct the test function let

$$\zeta_i(x) = \begin{cases} -\frac{\dot{V}_i}{2\pi} \ln(R_i/l) & \text{if } |x - X_i| < R_i, \\ -\frac{\dot{V}_i}{2\pi} \ln(|x - X_i|/l) & \text{if } R_i < |x - X_i| < l, \\ 0 & \text{else,} \end{cases}$$

See Figure 11. The test function ζ_i is a harmonic function such that the mass flux across the i -th droplet boundary is equal to \dot{V}_i :

$$\int_{B(X_i, R_i)} -\nabla \zeta_i(x) \cdot \left(\frac{x - X_i}{|x - X_i|} \right) dx = \dot{V}_i.$$

Now consider the test function $\zeta = \sum \lambda_i \zeta_i$ where the constants λ_1 and λ_2 need to be determined. (In case of additional droplets that lie in the support of ζ it would need to

be modified near the droplets as in (4.41).) One computes

$$\int -m(h(x))|\nabla\zeta(x)|^2 + 2\Delta h_v(x)\zeta(x) dx = \frac{1}{2\pi} \sum_{i=1}^2 (\dot{V}_i)^2 \ln(l/R_i) (-\lambda_i^2 + 2\lambda_i).$$

Maximizing in λ_i gives $\lambda_i = 1$. Therefore

$$\int m|\nabla\varphi_v(x)|^2 dx \geq \frac{1}{2\pi} \sum_{i=1}^2 \ln(l/R_i) (\dot{V}_i)^2 = \left(\frac{1}{2\pi} \sum_{i=1}^2 \ln(L/R_i) + O(1) \right) (\dot{V}_i)^2.$$

Upper bound. Let $l = L/3$, $\bar{X} = (X_1 + X_2)/2$ and $O = B(\bar{X}, L) \setminus (B(X_1, l) \cup B(X_2, l))$. We construct the test flux J as follows:

$$J(x) = \begin{cases} \dot{V}_1 J_1(x - X_1) & \text{if } x \in B(X_1, l), \\ \dot{V}_2 J_2(x - X_2) & \text{if } x \in B(X_2, l), \\ J^{\text{out}} & \text{if } x \in O, \\ 0 & \text{if } x \notin B(\bar{X}, L), \end{cases} \quad (4.37)$$

where J_i for $i = 1, 2$ were defined above and $J^{\text{out}} = -\nabla\mu_{\text{out}}$ with

$$-\Delta\mu_{\text{out}} = 0 \quad \text{on } O,$$

$-\nabla\mu_{\text{out}} \cdot \nu = \frac{\dot{V}_i}{2\pi l}$ on $\partial B(X_i, l)$ for $i = 1, 2$, and $\nabla\mu_{\text{out}} \cdot \nu = 0$ on $\partial B(\bar{X}, L)$. Note that boundary conditions are such that $J_i \cdot \nu = J^{\text{out}} \cdot \nu$ at $\partial B(X_i, l)$, which makes J an admissible test function.

Scaling of the domain and changing variables shows that

$$\int_O |\nabla\mu_{\text{out}}|^2 dx$$

is independent of L , which is the only length scale in the problem. Therefore for some C , independent of L and V_i for $i = 1, 2$,

$$\int_O \frac{1}{m(h)} |J^{\text{out}}|^2 \leq C.$$

Combining this bound with the ones in (4.33) and (4.34) yields the desired upper bound.

4.3.2 Computing G^m

Let $\dot{X}, \dot{Y} \in \mathbb{R}^2$. To compute the diagonal elements, consider the change vectors $v_1 := (0_2, \dot{X}^T, 0_2)^T$ and $v_2 := (0_2, \dot{Y}^T, 0_2)^T$ that perturb the location of X_1 . By the definition of the dissipation rate (4.12)

$$\dot{X}^T G_{11}^m \dot{Y} = \int_{\mathbb{R}^2} m \nabla\varphi_{v_1} \cdot \nabla\varphi_{v_2} dx,$$

where φ_{v_i} solve

$$\begin{aligned}\nabla(m\nabla\varphi_{v_1}) &= -\nabla h_1 \cdot \dot{X}, \\ \nabla(m\nabla\varphi_{v_2}) &= -\nabla h_1 \cdot \dot{Y},\end{aligned}\tag{4.38}$$

and $\nabla\varphi_{v_i} \cdot v \rightarrow 0$ as $|x| \uparrow \infty$.

The difference between φ_{v_1} and $\Psi_{1,V_1}^{\dot{X}}$ (defined in (4.8)) – besides the shift to the origin – stems from different mobilities: $\Psi_{1,V_1}^{\dot{X}}$ solves the same problem, but with $m = m(h_\theta)$ replaced by $m_1(x) = m(1 + h_1(x))$. Nevertheless, we justify below that φ_{v_1} can be approximated by $\Psi_{1,V_1}^{\dot{X}}$, so that we can replace $\varphi_{v_1}(x + X_1)$ by $\Psi_{1,V_1}^{\dot{X}}(x) = \Psi_{1,V_1}(|x|) \frac{x}{|x|} \cdot \dot{X}$.

Below we also use the following: Let $\zeta \in C([0, \infty), [0, \infty))$ and $\int_0^\infty \zeta(r)r^3 dr < \infty$. Elementary calculation verifies that

$$\int_{\mathbb{R}^2} \zeta(|x|)(\dot{X} \cdot x)(\dot{Y} \cdot x) dx = \frac{\dot{X} \cdot \dot{Y}}{2} \int_{\mathbb{R}^2} \zeta(|x|) |x|^2 dx.$$

In the following we use that $h_{V_1,0}$ is a radially symmetric function and denote the function of the radial distance by the same symbol. Assuming for now the validity of the approximation of φ_{v_i} by Ψ_{1,V_1} (justified below), after integration by parts one obtains:

$$\begin{aligned}\dot{X}^T G_{11}^m \dot{Y} &\approx \int_{\mathbb{R}^2} \left(\Psi_{1,V_1}(|x|) \frac{x}{|x|} \cdot \dot{X} \right) (\nabla h_{V_1,0}(x) \cdot \dot{Y}) dx \\ &= \frac{\dot{X} \cdot \dot{Y}}{2} \int_{\mathbb{R}^2} \Psi_{1,V_1}(|x|) \frac{x}{|x|} \cdot \partial_r h_{V_1,0}(|x|) \frac{x}{|x|} dx \\ &= \dot{X} \cdot \dot{Y} \int_{\mathbb{R}^2} \Psi_{1,V_1}(|x|) \frac{x_1}{|x|} \partial_r h_{V_1,0}(|x|) \frac{x_1}{|x|} dx \\ &= \dot{X} \cdot \dot{Y} \int_{\mathbb{R}^2} \Psi_{1,V_1}(|x|) \frac{x_1}{|x|} \partial_1 h_{V_1,0}(x) dx \\ &= \dot{X} \cdot \dot{Y} \int_{\mathbb{R}^2} m_1 |\nabla \Psi_{1,V_1}(x)|^2 dx.\end{aligned}\tag{4.39}$$

Thus $G_{11}^m \approx \text{diag}(g_1, g_1)$ with

$$g_1 = \int_{\mathbb{R}^2} m_1 |\nabla \Psi_{1,V_1}(x)|^2 dx.$$

G_{22}^m is computed analogously.

To determine G_{12}^m , consider the change vectors $v_1 := (0_2, \dot{X}^T, 0_2)^T$ and $v_2 := (0_4, \dot{Y}^T)^T$. Then

$$\dot{X}^T G_{12}^m \dot{Y} = \int_{\mathbb{R}^2} m \nabla \varphi_{v_1} \cdot \nabla \varphi_{v_2} dx.$$

In (4.51) we justify that

$$|\dot{X}^T G_{12}^m \dot{Y}| = \left| \int_{B(X_2, R_2)} \varphi_{v_1}(x) \nabla h_{V_2,0}(x) \cdot \dot{Y} dx \right| = |\dot{X}| |\dot{Y}| o(\sqrt{g_1 g_2}).\tag{4.40}$$

Justification of the approximations. We introduce the following, intermediate, approximation of φ_{v_1} : Choose $R_2 \ll l \ll L$. Let $\xi \in C^\infty([0, \infty), [0, 1])$ be a cut-off function supported on $[0, 2]$ and equal to 1 on $[0, 1]$. Let $\xi_l(x) := \xi(|x|/l)$. Then define

$$\tilde{\varphi}_{v_1} := (1 - \xi_l(x - X_2))\Psi_{1, V_1}^{\dot{X}}(x - X_1) + \xi_l(x - X_2)\Psi_{1, V_1}^{\dot{X}}(X_2 - X_1). \quad (4.41)$$

Let us denote the error term by $\varphi_e := \varphi_{v_1} - \tilde{\varphi}_{v_1}$. Let A be the annulus $B(X_2, 2l) \setminus \bar{B}(X_2, l)$. Let

$$f := -\nabla \cdot (m\nabla\varphi_e). \quad (4.42)$$

Note that $f = 0$ on $\mathbb{R}^2 \setminus A$, and that on A

$$f = -\Delta\xi_l(x - X_2)(\Psi_{1, V_1}^{\dot{X}}(x - X_1) - \Psi_{1, V_1}^{\dot{X}}(X_2 - X_1)) - 2\nabla\xi_l(x - X_2) \cdot \nabla\Psi_{1, V_1}^{\dot{X}}(x - X_1).$$

Therefore on A

$$|f| \lesssim \frac{1}{l^2} \max_{x \in A} |\nabla\Psi_{1, V_1}^{\dot{X}}(x - X_1)| l + \frac{1}{l} \max_{x \in A} |\nabla\Psi_{1, V_1}^{\dot{X}}(x - X_1)|.$$

The dipolar form (4.9) of $\Psi_{1, V_1}^{\dot{X}}$ and the scaling (3.28) imply via (3.30) that for $|z| > R_1$

$$|\Psi_{1, V_1}^{\dot{X}}(z)| \lesssim |\dot{X}| \frac{1}{|z|} V_1^\gamma \beta(V_1). \quad (4.43)$$

Here $\gamma = \max\{3 - q, 1\}/3$, $\beta(V) = \ln V$ if $q = 2$ and $\beta \equiv 1$ otherwise. Via (3.23) it then follows

$$|\nabla\Psi_{1, V_1}^{\dot{X}}(z)| \lesssim |\dot{X}| \left(\partial_r \Psi_{1, V_1}(|z|) + \frac{1}{|z|} \Psi_{1, V_1}(|z|) \right) \lesssim |\dot{X}| \frac{1}{|z|^2} V_1^\gamma \beta(V_1) \quad (4.44)$$

for $|z| > |R_1|$. Using this estimate we obtain that on A

$$|f| \lesssim \frac{|\dot{X}|}{l} V_1^\gamma \beta(V_1) \frac{1}{L^2}. \quad (4.45)$$

Note that the decay of $\nabla\tilde{\varphi}_{v_1}$ implies that

$$\int_{\mathbb{R}^2} -\nabla h_1 \cdot \dot{X} - f \, dx = \lim_{r \rightarrow \infty} \int_{B(0, r)} \nabla \cdot (m\nabla\tilde{\varphi}_{v_1}) \, dx = \lim_{r \rightarrow \infty} \int_{\partial B(0, r)} \partial_\nu (m\nabla\tilde{\varphi}_{v_1}) \, dx = 0$$

Thus

$$\int_{\mathbb{R}^2} f \, dx = 0.$$

Let $B_A := B(X_2, 2l)$. Note that $\text{supp } f \subset B_A$. Let $\bar{\varphi}_e := \int_{B_A} \varphi_e dx$. Multiplying (4.42) by $\varphi_e(x)$ and integrating by parts gives

$$\int_{\mathbb{R}^2} m |\nabla \varphi_e|^2 dx = \int_{\mathbb{R}^2} f(x) \varphi_e(x) - f(x) \bar{\varphi}_e dx \leq \|f\|_{L^2(B_A)} \|\varphi_e - \bar{\varphi}_e\|_{L^2(B_A)}. \quad (4.46)$$

By Poincare inequality

$$\|\varphi_e - \bar{\varphi}_e\|_{L^2(B_A)}^2 \lesssim l^2 \int_{B_A} m |\nabla \varphi_e|^2 dx. \quad (4.47)$$

Combining the inequalities gives

$$\int_{\mathbb{R}^2} m |\nabla \varphi_e|^2 dx \lesssim l^2 \|f\|_{L^2(B_A)}^2. \quad (4.48)$$

We also utilize the following estimate: Recall from (4.8) and (4.9) that

$$\nabla \cdot (m_1(x - X_1) \nabla \Psi_{1, V_1}^{\dot{Y}}(x - X_1)) = -\nabla h_1 \cdot \dot{Y}.$$

Consequently, using that $m(x) \geq m_1(x - X_1)$, we obtain

$$\begin{aligned} \int_{\mathbb{R}^2} m |\nabla \varphi_{v_2}|^2 dx &= \min_J \left\{ \int_{\mathbb{R}^2} \frac{1}{m} |J|^2 : \nabla \cdot J = \nabla h_1 \cdot \dot{Y} \right\} \\ &\leq \min_J \left\{ \int_{\mathbb{R}^2} \frac{1}{m_1} |J(\cdot + X_1)|^2 : \nabla \cdot J = \nabla h_1 \cdot \dot{Y} \right\} \\ &= \int_{\mathbb{R}^2} m_1 |\nabla \Psi_{1, V_1}^{\dot{Y}}|^2 = g_1 |\dot{Y}|^2 \end{aligned} \quad (4.49)$$

We are finally ready to justify the approximation used in (4.39)

$$\begin{aligned} \dot{X}^T G_{11}^m \dot{Y} &= \int_{\mathbb{R}^2} m \nabla \varphi_{v_1} \cdot \nabla \varphi_{v_2} dx \\ &= \int_{\mathbb{R}^2} m \nabla \tilde{\varphi}_{v_1} \cdot \nabla \varphi_{v_2} dx + \int_{\mathbb{R}^2} m \nabla \varphi_e \cdot \nabla \varphi_{v_2} dx \\ &= \int_{\mathbb{R}^2} \Psi_{1, V_1}^{\dot{X}} \nabla h_{V_1, 0}(x) \cdot Y dx + \int_{\mathbb{R}^2} m \nabla \varphi_e \cdot \nabla \varphi_{v_2} dx \end{aligned}$$

To conclude we use (4.48), (4.45) and (4.20) to estimate:

$$\begin{aligned} \left| \int_{\mathbb{R}^2} m \nabla \varphi_e \cdot \nabla \varphi_{v_2} dx \right| &\leq \left(\int_{\mathbb{R}^2} m |\nabla \varphi_e|^2 dx \right)^{\frac{1}{2}} \left(\int_{\mathbb{R}^2} m |\nabla \varphi_{v_2}|^2 dx \right)^{\frac{1}{2}} \\ &\lesssim l \|f\|_{L^2(B_A)} \sqrt{g_1} |\dot{Y}| \\ &\lesssim ll \frac{|\dot{X}|}{l} V_1^\gamma \beta(V_1) \frac{1}{L^2} \sqrt{g_1} |\dot{Y}| \\ &\ll |\dot{X}| |\dot{Y}| V_1^{(2-q)/3} \beta(V_1) \sqrt{g_1} \lesssim |\dot{X}| |\dot{Y}| g_1. \end{aligned} \quad (4.50)$$

We now turn to showing (4.40).

$$\begin{aligned}
\int_{\mathbb{R}^2} m \nabla \varphi_{v_1} \cdot \nabla \varphi_{v_2} dx &= \int_{\mathbb{R}^2} m \nabla \tilde{\varphi}_{v_1} \cdot \nabla \varphi_{v_2} dx + \int_{\mathbb{R}^2} m \nabla \varphi_e \cdot \nabla \varphi_{v_2} dx \\
&= \int_{\mathbb{R}^2} \tilde{\varphi}_{v_1} \nabla h_2 \cdot \dot{Y} dx + \int_{\mathbb{R}^2} m \nabla \varphi_e \cdot \nabla \varphi_{v_2} dx \\
&= \int_{\mathbb{R}^2} m \nabla \varphi_e \cdot \nabla \varphi_{v_2} dx
\end{aligned}$$

since $\tilde{\varphi}_{v_1}$ is constant on $B(X_2, R_2)$. The remaining estimate is similar to (4.50):

$$\begin{aligned}
\left| \int_{\mathbb{R}^2} m \nabla \varphi_e \cdot \nabla \varphi_{v_2} dx \right| &\leq \left(\int_{\mathbb{R}^2} m |\nabla \varphi_e|^2 dx \right)^{\frac{1}{2}} \left(\int_{\mathbb{R}^2} m |\nabla \varphi_{v_2}|^2 dx \right)^{\frac{1}{2}} \\
&\lesssim l l \frac{|\dot{X}|}{l} V_1^\gamma \beta(V_1) \frac{1}{L^2} \sqrt{g_1} |\dot{Y}| \\
&\ll |\dot{X}| |\dot{Y}| V_1^{(2-q)/3} \beta(V_1) \sqrt{g_2} \lesssim |\dot{X}| |\dot{Y}| \sqrt{g_1 g_2}.
\end{aligned} \tag{4.51}$$

4.3.3 Computing C

Consider the change vectors $v_1 := (0_2, \dot{X}^T, 0_2)^T$ and $v_2 := (1, -1, 0_4)^T$.

$$\begin{aligned}
\dot{X}^T [C_{11}, C_{12}] \begin{pmatrix} 1 \\ -1 \end{pmatrix} &= \int_{\mathbb{R}^2} m(h) \nabla \varphi_{v_1}(x) \cdot \nabla \varphi_{v_2}(x) dx \\
&= - \int \varphi_{v_1} \left(\frac{\partial h_1}{\partial V_1}(x) - \frac{\partial h_2}{\partial V_2}(x) \right) dx \\
&\stackrel{\text{using (4.57)}}{\approx} - \int \tilde{\varphi}_{v_1} \left(\frac{\partial h_1}{\partial V_1}(x) - \frac{\partial h_2}{\partial V_2}(x) \right) dx \\
&= \int_{B(X_2, R_2)} \Psi_{1, V_1}(|X_2 - X_1|) \frac{X_2 - X_1}{|X_2 - X_1|} \cdot \dot{X} \frac{\partial h_2}{\partial V_2} dx \\
&= \Psi_{1, V_1}(|X_2 - X_1|) \frac{X_2 - X_1}{|X_2 - X_1|} \cdot \dot{X}.
\end{aligned}$$

Thus

$$C_{11} - C_{12} \approx \Psi_{1, V_1}(|X_2 - X_1|) \frac{X_2 - X_1}{|X_2 - X_1|} \approx \lim_{r \rightarrow \infty} r \Psi_{1, V_1}(r) \frac{X_2 - X_1}{|X_2 - X_1|^2}.$$

As above, this is the only requirement on C_{11} and C_{12} . We set $C_{11} = 0$ and thus

$$C_{12} \approx - \lim_{r \rightarrow \infty} r \Psi_{1, V_1}(r) \frac{X_2 - X_1}{|X_2 - X_1|^2}.$$

Justification of the approximation. To validate the approximations used in computing the matrix C we need to refine the approximation of φ_{v_1} . Analogously to (4.9) we

define

$$\Psi_{0,V}^{\dot{X}}(x) = \Psi_{0,V}(|x|) |\dot{X}| \cos \theta \quad \text{where } \cos \theta = \frac{x}{|x|} \cdot \frac{\dot{X}}{|\dot{X}|}. \quad (4.52)$$

Let $Z = \nabla \Psi_{1,V_1}^{\dot{X}}(X_2 - X_1)$. The construction is the refinement of the one in Subsection 4.3.2. Let

$$\tilde{\varphi}_{v_1} := (1 - \xi_l(x - X_2)) \Psi_{1,V_1}^{\dot{X}}(x - X_1) + \xi_l(x - X_2) (\Psi_{1,V_1}^{\dot{X}}(X_2 - X_1) + \Psi_{0,V_1}^Z(x - X_2)). \quad (4.53)$$

Let $\varphi_e := \varphi_{v_1} - \tilde{\varphi}_{v_1}$. Then $f = -\nabla \cdot (m \nabla \varphi_e)$ is supported on annulus $A = B(X_2, 2l) \setminus \bar{B}(X_2, l)$. On A

$$\begin{aligned} f &= -\Delta(\varphi_{v_1} - \tilde{\varphi}_{v_1}) = -\Delta \tilde{\varphi}_{v_1} \\ &= -\Delta \xi_l \left(\Psi_{1,V_1}^{\dot{X}}(x - X_1) - \Psi_{1,V_1}^{\dot{X}}(X_2 - X_1) + \Psi_{0,V_1}^Z(x - X_2) \right) \\ &\quad - \nabla \xi_l (\nabla \Psi_{1,V_1}^{\dot{X}}(x - X_1) - \nabla \Psi_{0,V_1}^Z(x - X_2)). \end{aligned}$$

To estimate f we use (4.52) and the form of $\Psi_{0,V_1}(|x - X_2|)$ given in (B 15), (B 20) and (B 24). More precisely on A :

$$\begin{aligned} |\Psi_{0,V_1}^Z(x - X_2) - Z \cdot (x - X_2)| &\lesssim \frac{R_2^2}{l}, \\ |\nabla \Psi_{0,V_1}^Z(x - X_2) - Z| &\lesssim \frac{R_2^2}{l^2}. \end{aligned}$$

We furthermore use an extension of (4.43) in a form valid on A :

$$|D^2 \Psi_{1,V_1}^{\dot{X}}| \lesssim |\dot{X}| \frac{1}{L^3} V_1^\gamma \beta(V_1).$$

These estimates imply that

$$|f| \lesssim |\dot{X}| \frac{1}{L^3} V_1^\gamma \beta(V_1) \left(1 + \frac{R_2^2 L}{l^3} \right) \lesssim |\dot{X}| \frac{1}{L^3} V_1^\gamma \beta(V_1) \quad (4.54)$$

provided that we choose

$$l^3 \geq LR_2^2. \quad (4.55)$$

Let $B = B(X_1, 2L)$. From (4.48) we obtain via Poincaré inequality

$$\int_B \left| \varphi_e - \int_B \varphi_e \right|^2 dx \lesssim L^2 l^2 \|f\|_{L^2(B_A)}^2. \quad (4.56)$$

We are now ready to estimate the error in computing C . Using that $\int_{\mathbb{R}^2} \frac{\partial h_1}{\partial V_1} - \frac{\partial h_2}{\partial V_2} = 0$,

$$\begin{aligned}
\left| \int_{\mathbb{R}^2} (\varphi_{v_1} - \tilde{\varphi}_{v_1}) \left(\frac{\partial h_1}{\partial V_1} - \frac{\partial h_2}{\partial V_2} \right) dx \right| &= \left| \int_{\mathbb{R}^2} (\varphi_e - \int_B \varphi_e) \left(\frac{\partial h_1}{\partial V_1} - \frac{\partial h_2}{\partial V_2} \right) dx \right| \\
&\leq \left(\int_B \left| \varphi_e - \int_B \varphi_e \right|^2 dx \right)^{\frac{1}{2}} \left(\int_B \left| \frac{\partial h_1}{\partial V_1} \right|^2 + \left| \frac{\partial h_2}{\partial V_2} \right|^2 dx \right)^{\frac{1}{2}} \\
&\lesssim lL \|f\|_{L^2(B_A)} (V_1^{-\frac{1}{3}} + V_2^{-\frac{1}{3}}) \\
&\lesssim \frac{|\dot{X}|}{L} V_1^\gamma \beta(V_1) \frac{l^2}{L} \left(\frac{1}{R_1} + \frac{1}{R_2} \right) \\
&\ll \frac{|\dot{X}|}{L} V_1^\gamma \beta(V_1) \lesssim |\dot{X}| \Psi_{1,V_1}(|X_2 - X_1|) \tag{4.57}
\end{aligned}$$

provided that

$$l^2 \ll LR_1 \text{ and } l^2 \ll LR_2.$$

It is important to note that l can be chosen to satisfy both this requirement and (4.55), provided that R_1 and R_2 are of comparable size. More precisely if

$$\left(\frac{R_2}{R_1} \right)^3 \ll \frac{L}{R_2}.$$

Acknowledgements

Karl Glasner acknowledges support under NSF award DMS-0405596 and thanks the University of Bonn for their hospitality. Felix Otto acknowledges partial support by the Sonderforschungsbereich 611 *Singular phenomena and scaling in mathematical models* at Bonn University. Tobias Rump acknowledges support by the Sonderforschungsbereich 611. Dejan Slepčev would like to thank University of Bonn for hospitality and acknowledge the support from NSF through the grants DMS-0638481 and DMS-0405343. The authors would also like to thank the referees for helpful suggestions.

Appendix A: Analysis of ψ_1

We start with the asymptotics in (3.27) which are easier to establish because of the variational characterization and its dual:

$$\begin{aligned}
&\frac{1}{2} \int \bar{m} |\nabla \psi_1|^2 dx \\
&= \max_{\psi_1} \left\{ -\frac{1}{2} \int \bar{m} |\nabla \psi_1|^2 dx + \int \partial_1 \bar{h} \psi_1 dx \right\} \\
&= \min_J \left\{ \frac{1}{2} \int \frac{1}{\bar{m}} |J|^2 dx \mid -\partial_1 \bar{h} + \nabla \cdot J = 0 \right\}. \tag{A 1}
\end{aligned}$$

A.1 Case $q = 0$

The case of $q = 0$ and thus $\bar{m} \equiv 1$ however can be treated explicitly. For this purpose we turn to the formulation (3.22) which for the mesoscopic droplet profile (2.25) assumes the form

$$\begin{aligned} \sqrt{2} \frac{r}{R} - \partial_r^2 \psi_1 - \frac{1}{r} \partial_r \psi_1 + \frac{1}{r^2} \psi_1 &= 0 \quad \text{for } r < R, \\ -\partial_r^2 \psi_1 - \frac{1}{r} \partial_r \psi_1 + \frac{1}{r^2} \psi_1 &= 0 \quad \text{for } r > R, \\ \psi_1(r = 0) = 0, \quad \lim_{r \uparrow \infty} \partial_r \psi_1 &= 0. \end{aligned}$$

The solution of this ODE is easily checked to be

$$\psi_1 = \frac{R^2}{4\sqrt{2}} \begin{cases} -2\frac{r}{R} + \left(\frac{r}{R}\right)^3 & \text{for } r \leq R, \\ -\frac{R}{r} & \text{for } r \geq R \end{cases}. \quad (\text{A } 2)$$

Hence we obtain as claimed

$$\int \bar{m} |\nabla \psi_1|^2 dx = \int \partial_1 \bar{h} \psi_1 dx = \pi \int_0^\infty \partial_r \bar{h} \psi_1 r dr = \frac{\pi}{12} R^4.$$

A.2 Case $0 < q < 3$

For the range of $q \in (0, 3)$, we introduce the rescaling (which is consistent with (A 2) for $q = 0$)

$$\begin{aligned} x &= R\hat{x}, & \bar{h} &= R\hat{h}, & \bar{m} &= R^q \hat{m}, \\ \psi_1 &= R^{2-q} \hat{\psi}_1, & J &= R\hat{J}. \end{aligned} \quad (\text{A } 3)$$

Notice that with this rescaling, (A 1) turns into

$$\begin{aligned} R^{q-4} \frac{1}{2} \int \bar{m} |\nabla \psi_1|^2 dx & \\ &= \max_{\hat{\psi}_1} \left\{ -\frac{1}{2} \int \hat{m} |\hat{\nabla} \hat{\psi}_1|^2 d\hat{x} + \int \hat{\partial}_1 \hat{h} \hat{\psi}_1 d\hat{x} \right\} \\ &= \min_{\hat{J}} \left\{ \frac{1}{2} \int \frac{1}{\hat{m}} |\hat{J}|^2 d\hat{x} \mid -\hat{\partial}_1 \hat{h} + \hat{\nabla} \cdot \hat{J} = 0 \right\}. \end{aligned} \quad (\text{A } 4)$$

Recall the outcome of the analysis in Section 2 in the form of (2.23) and (2.24). It implies that in the rescaling of (A 3), $\bar{h} - 1$ converges to the mesoscopic profile $\bar{h}_{\text{meso}} - 1$ given in (2.25):

$$\hat{h} \rightarrow \begin{cases} \frac{1}{\sqrt{2}}(1 - \hat{r}^2) & \text{for } \hat{r} < 1, \\ 0 & \text{for } \hat{r} > 1 \end{cases} := \hat{h}_{\text{lim}}.$$

Because of $q > 0$, this entails

$$\hat{m} \rightarrow \begin{cases} \left(\frac{1}{\sqrt{2}}(1 - \hat{r}^2)\right)^q & \text{for } \hat{r} \leq 1, \\ 0 & \text{for } \hat{r} \geq 1 \end{cases} := \hat{m}_{\text{lim}}.$$

Hence we infer from (A 4)

$$\begin{aligned} & \liminf_{R \uparrow \infty} R^{q-4} \frac{1}{2} \int \bar{m} |\nabla \psi_1|^2 d\hat{x} \\ & \geq \max_{\hat{\psi}_1} \left\{ -\frac{1}{2} \int \hat{m}_{\text{lim}} |\hat{\nabla} \hat{\psi}_1|^2 dx + \int \hat{\partial}_1 \hat{h}_{\text{lim}} \hat{\psi}_1 d\hat{x} \right\} \end{aligned} \quad (\text{A } 5)$$

and

$$\begin{aligned} & \liminf_{R \uparrow \infty} R^{q-4} \frac{1}{2} \int \bar{m} |\nabla \psi_1|^2 dx \\ & \leq \min_j \left\{ \frac{1}{2} \int \frac{1}{\hat{m}_{\text{lim}}} |\hat{J}|^2 d\hat{x} \mid -\hat{\partial}_1 \hat{h}_{\text{lim}} + \hat{\nabla} \cdot \hat{J} = 0 \right\}, \end{aligned} \quad (\text{A } 6)$$

with the understanding that $\int \frac{1}{\hat{m}_{\text{lim}}} |\hat{J}|^2 d\hat{x} = +\infty$ if the support of \hat{J} is not contained in the support of \hat{m}_{lim} , i.e. the closed unit disk. It remains to argue that

$$\exists \hat{J} \text{ s. t. } \quad -\hat{\partial}_1 \hat{h}_{\text{lim}} + \hat{\nabla} \cdot \hat{J} = 0 \quad \text{and} \quad \int \frac{1}{\hat{m}_{\text{lim}}} |\hat{J}|^2 d\hat{x} < \infty. \quad (\text{A } 7)$$

Indeed, if this is the case, the variational problem on the r.h.s. of (A 6) has a (unique) solution \hat{J} . The first variation shows that \hat{J} is of the form $\hat{J} = -\hat{m}_{\text{lim}} \hat{\nabla} \hat{\psi}_1$ and that $\hat{\psi}_1$ solves the variational problem in (A 5). Hence (A 7) implies that (A 5) and (A 6) contract to

$$\begin{aligned} & \lim_{R \uparrow \infty} R^{q-4} \frac{1}{2} \int \bar{m} |\nabla \psi_1|^2 dx \\ & = \max_{\hat{\psi}_1} \left\{ -\frac{1}{2} \int \hat{m}_{\text{lim}} |\hat{\nabla} \hat{\psi}_1|^2 d\hat{x} + \int \hat{\partial}_1 \hat{h}_{\text{lim}} \hat{\psi}_1 d\hat{x} \right\} \\ & = \min_j \left\{ \frac{1}{2} \int \frac{1}{\hat{m}_{\text{lim}}} |\hat{J}|^2 d\hat{x} \mid -\hat{\partial}_1 \hat{h}_{\text{lim}} + \hat{\nabla} \cdot \hat{J} = 0 \right\}. \end{aligned}$$

We now remark that (A 7) is true for $q < 3$: Consider $\hat{J} = \hat{h}_{\text{lim}} - \binom{1}{0}$ which automatically satisfies the first condition in (A 7) and for which

$$\int \frac{1}{\hat{m}_{\text{lim}}} |\hat{J}|^2 d\hat{x} = \int \frac{(\hat{h}_{\text{lim}} - 1)^2}{\hat{m}_{\text{lim}}} d\hat{x} = 2\pi \int_0^1 \left(\frac{1}{\sqrt{2}} (1 - \hat{r}^2) \right)^{2-q} \hat{r} d\hat{r} < \infty,$$

provided $q < 3$. But since $\frac{1}{\hat{m}_{\text{lim}}} \hat{J} = \frac{1}{\hat{m}_{\text{lim}}} \hat{h}_{\text{lim}} - \binom{1}{0}$ is not a gradient, we obtain the strict inequality

$$\lim_{R \uparrow \infty} R^{q-4} \int \bar{m} |\nabla \psi_1|^2 dx < \int_{\{|\hat{x}| < 1\}} \left(\frac{1}{\sqrt{2}} (1 - |\hat{x}|^2) \right)^{2-q} d\hat{x},$$

as opposed to the analogous equality in the one-dimensional case. Notice that as in the one-dimensional case, the leading order behaviour depends only on the mesoscopic droplet profile.

A.3 Case $q > 3$

We reformulate (A 1) as

$$\begin{aligned} & \frac{1}{2} \int \bar{m} |\nabla \psi_1|^2 dx \\ &= \left\{ \begin{array}{l} \max_{\psi_1} \left\{ -\frac{1}{2} \int \bar{m} |\nabla \psi_1|^2 dx - \int (\bar{h} - 1) \partial_1 \psi_1 dx \right\} \\ \min_J \left\{ \frac{1}{2} \int \frac{1}{\bar{m}} |J + (\bar{h} - 1) \begin{pmatrix} 1 \\ 0 \end{pmatrix}|^2 dx \mid \nabla \cdot J = 0 \right\} \end{array} \right\}. \end{aligned} \quad (\text{A } 8)$$

Furthermore, we write (A 8) in polar coordinates, using the fact that ψ_1 is of the form (3.20) so that $J = -\bar{m} \nabla \psi_1 - (\bar{h} - 1) \begin{pmatrix} 1 \\ 0 \end{pmatrix}$ can be written as

$$J(x) = J_r(r) \begin{pmatrix} \cos \varphi \\ \sin \varphi \end{pmatrix} - J_\varphi(r) \begin{pmatrix} -\sin \varphi \\ \cos \varphi \end{pmatrix}.$$

Hence from (A 8) we obtain on the one hand

$$\begin{aligned} & \frac{1}{2\pi} \int_0^\infty \bar{m} |\nabla \psi_1|^2 dx \\ &= \max_{\psi_1(r)} \left\{ -\frac{1}{2} \int_0^\infty \bar{m} \left((\partial_r \psi_1)^2 + \left(\frac{\psi_1}{r} \right)^2 \right) r dr - \int_0^\infty (\bar{h} - 1) \partial_r \psi_1 r dr \right\} \end{aligned} \quad (\text{A } 9)$$

and on the other hand

$$\begin{aligned} & \frac{1}{2\pi} \int_0^\infty \bar{m} |\nabla \psi_1|^2 dx \\ &= \min_{J_r(r), J_\varphi(r)} \left\{ \frac{1}{2} \int_0^\infty \frac{1}{\bar{m}} \left((J_r + (\bar{h} - 1))^2 + (J_\varphi + (\bar{h} - 1))^2 \right) r dr \mid \partial_r J_r + \frac{1}{r} J_r - \frac{1}{r} J_\varphi = 0 \right\} \\ &= \min_{J_r(r)} \left\{ \frac{1}{2} \int_0^\infty \frac{1}{\bar{m}} \left((J_r + (\bar{h} - 1))^2 + (r \partial_r J_r + J_r + (\bar{h} - 1))^2 \right) r dr \right\}. \end{aligned} \quad (\text{A } 10)$$

We employ the non-linear rescaling (2.12) used for the foot region in Section 2

$$r = R \exp\left(\frac{s}{R}\right), \quad J_r = R^{-1} \hat{J}_r,$$

(A 9) and (A 10) turn into

$$\begin{aligned} & \frac{1}{2\pi R} \int \bar{m} |\nabla \psi_1|^2 dx \\ &= \max_{\psi_1(s)} \left\{ -\frac{1}{2} \int_{-\infty}^{+\infty} \bar{m} \left((\partial_s \psi_1)^2 + R^{-2} \psi_1^2 \right) ds - \int_{-\infty}^{+\infty} (\bar{h} - 1) \partial_s \psi_1 \exp\left(\frac{s}{R}\right) ds \right\} \\ &= \min_{\hat{J}_r(s)} \left\{ \frac{1}{2} \int_{-\infty}^{+\infty} \frac{1}{\bar{m}} \left((R^{-1} \hat{J}_r + (\bar{h} - 1))^2 + (\partial_s \hat{J}_r + R^{-1} \hat{J}_r + (\bar{h} - 1))^2 \right) \exp\left(2\frac{s}{R}\right) ds \right\}. \end{aligned} \quad (\text{A } 11)$$

We recall from (2.15) that to leading order, \bar{h} is characterized by

$$\int_{\bar{h}(s)}^2 \frac{1}{\sqrt{2W(h)}} dh = s \quad \text{for } |s| \ll R.$$

Hence the (pointwise) limits $\bar{h}_{\text{lim}}(s)$ and \bar{m}_{lim} of $\bar{h}(s)$ and $\bar{m}(s)$, respectively, for $R \uparrow \infty$ are characterized by

$$\int_{\bar{h}_{\text{lim}}(s)}^2 \frac{1}{\sqrt{2U(h)}} dh = s \quad \text{and} \quad \bar{m}_{\text{lim}}(s) = \bar{h}_{\text{lim}}(s)^p \quad \text{for all } s.$$

This entails the differential characterization

$$\partial_s \bar{h}_{\text{lim}} = -\sqrt{2U(\bar{h}_{\text{lim}})} \quad \text{and} \quad \lim_{s \uparrow -\infty} \bar{h}_{\text{lim}} = +\infty, \quad \lim_{s \uparrow \infty} \bar{h}_{\text{lim}} = 1.$$

Thus we obtain from (A 11)

$$\begin{aligned} & \max_{\psi_1(s)} \left\{ -\frac{1}{2} \int_{-\infty}^{+\infty} \bar{m}_{\text{lim}} (\partial_s \psi_1)^2 ds - \int_{-\infty}^{+\infty} (\bar{h}_{\text{lim}} - 1) \partial_s \psi_1 ds \right\} \\ & \leq \liminf_{R \uparrow \infty} \frac{1}{2\pi R} \int \bar{m} |\nabla \psi_1|^2 dx \\ & \leq \limsup_{R \uparrow \infty} \frac{1}{2\pi R} \int \bar{m} |\nabla \psi_1|^2 dx \\ & \leq \min_{\hat{J}_r(s)} \left\{ \frac{1}{2} \int_{-\infty}^{+\infty} \frac{1}{\bar{m}_{\text{lim}}} ((\bar{h}_{\text{lim}} - 1)^2 + (\partial_s \hat{J}_r + (\bar{h}_{\text{lim}} - 1))^2) ds \right\}. \end{aligned} \quad (\text{A } 12)$$

Elementary optimization shows that the l.h.s. and r.h.s. coincide:

$$\begin{aligned} & \max_{\psi_1(s)} \left\{ -\frac{1}{2} \int_{-\infty}^{+\infty} \bar{m}_{\text{lim}} (\partial_s \psi_1)^2 ds - \int_{-\infty}^{+\infty} (\bar{h}_{\text{lim}} - 1) \partial_s \psi_1 ds \right\} \\ & = \frac{1}{2} \int_{-\infty}^{\infty} \frac{(\bar{h}_{\text{lim}} - 1)^2}{\bar{m}_{\text{lim}}} ds \\ & = \min_{\hat{J}_r(r)} \left\{ \frac{1}{2} \int_{-\infty}^{+\infty} \frac{1}{\bar{m}_{\text{lim}}} ((\bar{h}_{\text{lim}} - 1)^2 + (\partial_s \hat{J}_r + (\bar{h}_{\text{lim}} - 1))^2) ds \right\}. \end{aligned} \quad (\text{A } 13)$$

From (A 12) and (A 13) we thus obtain

$$\lim_{R \uparrow \infty} \frac{1}{R} \int \bar{m} |\nabla \psi_1|^2 dx = \pi \int_{-\infty}^{\infty} \frac{(\bar{h}_{\text{lim}} - 1)^2}{\bar{m}_{\text{lim}}} ds, \quad (\text{A } 14)$$

which implies the scaling claimed in (3.27) for $q > 3$. Notice that this deviates by a factor $\frac{1}{2}$ from the local expression

$$\lim_{R \uparrow \infty} \frac{1}{R} \int \frac{(\bar{h} - \bar{h}_{\infty})^2}{\bar{m}} dx = 2\pi \int_{-\infty}^{\infty} \frac{(\bar{h}_{\text{lim}} - 1)^2}{\bar{m}_{\text{lim}}} ds. \quad (\text{A } 15)$$

As in the one-dimensional case, the actual value depends on the details of the potential U , as can be seen from (D 4):

$$\pi \int_{-\infty}^{\infty} \frac{(\bar{h}_{\text{lim}} - 1)^2}{\bar{m}_{\text{lim}}} ds = \pi \int_1^{\infty} \frac{h-1}{h^q} \frac{1}{\sqrt{2U(h)}} dh.$$

A.4 Case $q = 3$

Guided by the prior analysis, we construct test functions for (A 9) and (A 1) which give identical bounds in terms of scaling in $R \gg 1$. For (A 9) we make the Ansatz

$$\psi_1 = \begin{cases} -\frac{1}{\sqrt{2}} \frac{r}{R} \frac{1}{\sqrt{2(R-r)+1}} & \text{for } r \leq R, \\ -\frac{1}{\sqrt{2}} \frac{R}{r} & \text{for } r \geq R \end{cases}.$$

This function is constructed such that its derivative

$$\partial_r \psi_1 = \begin{cases} -(1 + \frac{1}{\sqrt{2}R}) \frac{1}{(\sqrt{2(R-r)+1})^3} & \text{for } r \leq R, \\ \frac{1}{\sqrt{2}} \frac{R}{r^2} & \text{for } r \geq R \end{cases}$$

satisfies $\bar{m} \partial_r \psi_1 \approx -\bar{h}$ in the foot region. As in the one-dimensional case for $q = 3$, the main contribution comes from a logarithmic divergence in the foot region. Hence we right away use the mesoscopic droplet profile (2.25). We obtain for the various contributions to (A 9) in the regime $R \gg 1$

$$\begin{aligned} \int_0^R \bar{m} (\partial_r \psi_1)^2 r dr &\approx \frac{R}{\sqrt{2}} \ln R, \\ - \int_0^R (\bar{h} - 1) \partial_r \psi_1 r dr &\approx \frac{R}{\sqrt{2}} \ln R, \\ \int_0^R \bar{m} \left(\frac{\psi_1}{r} \right)^2 r dr &\sim R \ll R \ln R, \end{aligned}$$

and outside the droplet

$$\int_R^{\infty} \left((\partial_r \psi_1)^2 + \left(\frac{\psi_1}{r} \right)^2 \right) r dr = \frac{1}{4} \ll R \ln R.$$

From (A 9) and this asymptotic behaviour of the test function ψ_1 we conclude

$$\frac{1}{2\pi} \int \bar{m} |\nabla \psi_1|^2 dx \gtrsim \frac{R}{2\sqrt{2}} \ln R. \quad (\text{A } 16)$$

For the upper bound corresponding to (A 16), we make the Ansatz

$$J_r = \begin{cases} \frac{R}{\sqrt{2}} \left(\frac{r}{R} \right)^2 \left(1 - \frac{r}{R} \right)^2 & \text{for } r \leq R, \\ 0 & \text{for } r \geq R \end{cases}.$$

This radial flux component is constructed such that

$$\partial_r J_r = \begin{cases} \sqrt{2} \frac{r}{R} \left(1 - \frac{r}{R}\right) \left(1 - 2\frac{r}{R}\right) & \text{for } r \leq R, \\ 0 & \text{for } r \geq R \end{cases}$$

has the behaviour $r\partial_r J_r \approx -\sqrt{2}(R-r) \approx -(\bar{h}-1)$ in the foot region $r \approx R$. We turn to the individual terms in (A 10). In the regime $R \gg 1$ we have

$$\begin{aligned} \int_0^\infty \frac{1}{\bar{m}} (\bar{h}-1)^2 r dr &\approx \frac{R}{\sqrt{2}} \ln R, \\ \int_0^\infty \frac{1}{\bar{m}} (r\partial_r J_r + (\bar{h}-1))^2 r dr &\leq \int_0^R \frac{1}{(\bar{h}-1)^3} (r\partial_r J_r + (\bar{h}-1))^2 r dr \\ &\sim R \ll R \ln R, \\ \int_0^\infty \frac{1}{\bar{m}} J_r^2 r dr &\leq \int_0^R \frac{1}{(\bar{h}-1)^3} J_r^2 r dr \\ &\sim R \ll R \ln R. \end{aligned}$$

Combining these estimates with the help of the triangle inequality, we obtain

$$\frac{1}{2} \int \frac{1}{\bar{m}} ((J_r + (\bar{h}-1))^2 + (r\partial_r J_r + J_r + (\bar{h}-1))^2) r dr \lesssim \frac{R}{2\sqrt{2}} \ln R,$$

so that (A 10) yields

$$\frac{1}{2\pi} \int \bar{m} |\nabla \psi_1|^2 dx \lesssim \frac{R}{2\sqrt{2}} \ln R.$$

This concludes the proof of (3.27).

Appendix B: Analysis of ψ_0

We now turn to showing the scaling of $\int \psi_0 \partial_1 \bar{h} dx$ claimed in (3.28). Although problem (3.16) for ψ_0 is variational, the expression (3.28) does not have an easy variational characterization as (A 1). This means that we have to get an understanding of the solution $\psi_0(x)$ of (3.16), or in its radial version (3.21) for $\psi_0(r)$, itself.

Let us clearly state that we do not find universal functions $C_q(R)$ and $\hat{\psi}_0(\frac{r}{R})$, such that $\psi_0(r) = C_q(R) \hat{\psi}_0(\frac{r}{R})$ on the whole domain. Depending on the mobility exponent q , equations (B 18), (B 26) and (B 22) give asymptotic expressions for ψ_0 in the precursor, foot and cap region.

B.1 Case $q = 0$

When $q = 0$ (3.16) turns into

$$-\Delta \psi_0 = 0, \quad \nabla \psi_0 \rightarrow \begin{pmatrix} 1 \\ 0 \end{pmatrix} \quad \text{as } |x - X| \uparrow \infty,$$

so that (up to irrelevant additive constants):

$$\psi_0 = (x - X) \cdot \begin{pmatrix} 1 \\ 0 \end{pmatrix}. \quad (\text{B } 1)$$

We therefore obtain as claimed

$$-\int \psi_0 \partial_1 \bar{h} dx = \int \partial_1 \psi_0 (\bar{h} - 1) dx \stackrel{(\text{B } 1)}{=} \int (\bar{h} - 1) dx \stackrel{(2.25)}{=} \frac{\pi}{4\sqrt{2}} R^3.$$

B.2 Reduced order equation: The u problem

In the general case, we start by analysing

$$u := \frac{d \ln \psi_0}{d \ln r} = \frac{r}{\psi_0} \frac{d\psi_0}{dr}, \quad r \in (0, \infty), \quad (\text{B } 2)$$

which is well defined according to (3.25). The merit of u is that it satisfies a *first-order* but non-linear ODE (a Riccati equation):

$$\frac{du}{ds} = -u^2 + q a u + 1, \quad (\text{B } 3)$$

where the new variable s and the coefficient a are defined by

$$s := \ln \frac{r}{R} = \ln r - \ln R \quad \text{and} \quad a := -\frac{d \ln \bar{h}}{ds}. \quad (\text{B } 4)$$

Notice that

$$\lim_{s \rightarrow -\infty} u \stackrel{(\text{B } 2), (\text{B } 4)}{=} \lim_{r \downarrow 0} \frac{r}{\psi_0} \frac{d\psi_0}{dr} = 1, \quad (\text{B } 5)$$

since $\frac{d\psi_0}{dr}(r = 0) \neq 0$ because of uniqueness for the ODE (3.21). Together with $a = -\frac{d \ln \bar{h}}{ds} = -\frac{r}{\bar{h}} \frac{d\bar{h}}{dr} \geq 0$, it follows in particular from (B 3) and (B 5) that

$$u \geq 1 \quad \text{for all } s. \quad (\text{B } 6)$$

Based on the mesoscopic droplet profile (2.25), we find for the coefficient a that

$$a = \begin{cases} 2 \frac{\exp(2s)}{1 - \exp(2s) + \frac{\sqrt{2}}{R}} & \text{for } s < 0, \\ 0 & \text{for } s > 0 \end{cases}.$$

To leading order in $R \gg 1$, this implies the following asymptotic behaviour in the cap

region, the foot region and the precursor, respectively:

$$a = \left\{ \begin{array}{ll} 2 \exp(2s) & \text{for } -s \gg 1, \\ \frac{1}{-s + \frac{1}{\sqrt{2R}}} & \text{for } 0 < -s \ll 1, \\ 0 & \text{for } s > 0 \end{array} \right\}. \quad (\text{B } 7)$$

B.2.1 Cap region $-s \gg 1$

In view of (B 7), we notice that for $-s \gg 1$, (B 3) behaves as $\frac{du}{ds} = -u^2 + 1$ for which $u = 1$ is unstable at $s \rightarrow -\infty$. Hence we can extract information from the boundary condition (B 5). To this purpose, we approximate (B 3) for $u \approx 1$ and $-s \gg 1$. We obtain in view of (B 7)

$$\frac{d(u-1)}{ds} = -2(u-1) + 2q \exp(2s) \quad \text{for } -s \gg 1.$$

All solutions of the linear ODE are given by

$$u = 1 + \frac{1}{2}q \exp(2s) + \text{const} \exp(-2s) \quad \text{for } -s \gg 1,$$

and because of (B 5), the only relevant one is

$$u = 1 + \frac{1}{2}q \exp(2s) \quad \text{for } -s \gg 1. \quad (\text{B } 8)$$

This expression approximates the solution of (B 3) in the cap region $-s \gg 1$. In particular, it is independent of R to leading order. Since a is independent of R to leading order for $-s \gg \frac{1}{R}$ (cf. (B 7)), we obtain

$$u \text{ is to leading order independent of } R \text{ for } -s \gg \frac{1}{R}. \quad (\text{B } 9)$$

B.2.2 Foot region $0 < -s \ll 1$

We now turn to the foot region $0 < -s \ll 1$. Since $a \gg 1$ in this region, we also expect $u \gg 1$ in view of (B 3) and (B 6) (we use $q > 0$ here). In view of (B 7), (B 3) is then well approximated by

$$\frac{du}{ds} = -u^2 + q \frac{1}{-s + \frac{1}{\sqrt{2R}}} u \quad \text{for } 0 < -s \ll 1.$$

All solutions are given by

$$u = \left\{ \begin{array}{ll} \frac{q-1}{\left(-s + \frac{1}{\sqrt{2R}}\right) \left(1 + \text{const} \left(-s + \frac{1}{\sqrt{2R}}\right)^{q-1}\right)} & \text{for } q \neq 1, \\ \frac{1}{\left(-s + \frac{1}{\sqrt{2R}}\right) \left(\text{const} - \ln \left(-s + \frac{1}{\sqrt{2R}}\right)\right)} & \text{for } q = 1 \end{array} \right\}. \quad (\text{B } 10)$$

We notice that for $\frac{1}{R} \ll -s \ll 1$, u asymptotically simplifies to

$$u = \left\{ \begin{array}{ll} \frac{q-1}{(-s)(1 + \text{const}(-s)^{q-1})} & \text{for } q \neq 1, \\ \frac{1}{(-s)(\text{const} - \ln(-s))} & \text{for } q = 1 \end{array} \right\} \quad \text{for } \frac{1}{R} \ll -s \ll 1.$$

Thus we infer from (B 9):

const in (B 10) is to leading order independent of R .

Therefore we may conclude from (B 10) the following asymptotic behaviour:

$$u = \left\{ \begin{array}{ll} \frac{q-1}{\left(-s + \frac{1}{\sqrt{2R}}\right)} & \text{for } q > 1, \\ \frac{1}{\left(-s + \frac{1}{\sqrt{2R}}\right) \ln \frac{1}{-s + \frac{1}{\sqrt{2R}}}} & \text{for } q = 1, \\ \frac{C}{\left(-s + \frac{1}{\sqrt{2R}}\right)^q} & \text{for } q \in (0, 1), \end{array} \right\} \quad \text{for } 0 < -s \ll 1, \quad (\text{B 11})$$

where $C > 0$ denotes a generic constant independent of R . Notice that these expressions are consistent with our initial assumption that $u \gg 1$ in the foot region.

B.2.3 Precursor region $s > 0$

We finally address the precursor region $s > 0$, where in view of (B 7), u satisfies the autonomous equation

$$\frac{du}{ds} = -u^2 + 1 \quad \text{for } s > 0.$$

All solutions $u > 1$ (cf. (B 6)) are of the form

$$u = \frac{1}{\tanh(s + \text{const})} \quad \text{for } s > 0.$$

In order to connect to (B 11) we must have to leading order in $R \gg 1$:

$$u = \left\{ \begin{array}{ll} \frac{1}{\tanh\left(s + \frac{1}{(q-1)\sqrt{2R}}\right)} & \text{for } q > 1, \\ \frac{1}{\tanh\left(s + \frac{\ln(\sqrt{2R})}{\sqrt{2R}}\right)} & \text{for } q = 1, \\ \frac{1}{\tanh\left(s + \frac{1}{C(\sqrt{2R})^q}\right)} & \text{for } q \in (0, 1) \end{array} \right\} \quad \text{for } s > 0. \quad (\text{B 12})$$

The asymptotic expressions (B 8), (B 11) and (B 12) for u allow us to reconstruct ψ_0 according to (B 2).

B.3 Case $q > 1$: Recovering ψ_0 from u

We recall that we just found that to leading order in $R \gg 1$:

$$u(s) = \left. \begin{cases} \frac{1}{\tanh\left(s + \frac{1}{(q-1)\sqrt{2R}}\right)} & \text{for } s > 0 \\ \frac{q-1}{-s + \frac{1}{\sqrt{2R}}} & \text{for } 1 \gg -s > 0, \\ 1 + \frac{1}{2}q \exp(2s) & \text{for } -s \gg 1, \end{cases} \right\} \quad (\text{B 13})$$

B.3.1 Precursor region $s > 0$

In order to pass from $u = \frac{d \ln \psi_0}{ds}$ to $\ln \psi_0$, we use the boundary condition on ψ_0 for $r \uparrow \infty$ and then work backwards. We recall (3.23) in form of

$$\psi_0 = r - \text{const} \frac{R^2}{r} \quad \text{for } r \geq R, \quad (\text{B 14})$$

which translates into

$$\ln \psi_0 = s + \ln R + \ln(1 - \text{const} \exp(-2s)).$$

This implies

$$\frac{d \ln \psi_0}{ds} = \frac{1 + \text{const} \exp(-2s)}{1 - \text{const} \exp(-2s)},$$

whereas (B 13) can be rewritten as (to leading order in $R \gg 1$)

$$\frac{d \ln \psi_0}{ds} = \frac{1 + \left(1 - \frac{\sqrt{2}}{(q-1)R}\right) \exp(-2s)}{1 - \left(1 - \frac{\sqrt{2}}{(q-1)R}\right) \exp(-2s)},$$

from which we read off that $\text{const} = 1 - \frac{\sqrt{2}}{(q-1)R}$. Therefore, (B 14) can be specified to

$$\psi_0 = r - \left(1 - \frac{\sqrt{2}}{(q-1)R}\right) \frac{R^2}{r} \quad \text{for } r \geq R. \quad (\text{B 15})$$

B.3.2 Foot region $0 < -s \ll 1$

We now turn to the foot region. From (B 13) we infer that $\ln \psi_0$ must be of the form

$$\ln \psi_0 = (q-1) \ln \frac{1}{-s + \frac{1}{\sqrt{2R}}} + \text{const} \quad \text{for } 1 \gg -s > 0,$$

or

$$\psi_0 = \frac{\text{const}}{\left(-s + \frac{1}{\sqrt{2R}}\right)^{q-1}} \quad \text{for } 1 \gg -s > 0.$$

Since for $|s| \ll 1$, $\frac{r}{R} = \exp(s) \approx 1 + s$, we obtain to leading order

$$\psi_0 = \frac{\text{const}}{\left(1 - \frac{r}{R} + \frac{1}{\sqrt{2}R}\right)^{q-1}} \quad \text{for } r \approx R \text{ with } r \leq R.$$

The matching with (B 15) determines the constant in the above

$$\psi_0 = \frac{\sqrt{2}}{q-1} \frac{1}{(\sqrt{2}(R-r)+1)^{q-1}} \quad \text{for } r \approx R \text{ with } r \leq R. \quad (\text{B } 16)$$

B.3.3 Cap region $-s \gg 1$

We finally turn to the cap region. From (B 13) we gather that

$$\begin{aligned} \ln \psi_0 &= s + \frac{1}{4}q \exp(2s) + \text{const} \\ &= \ln \frac{r}{R} + \frac{1}{4}q \left(\frac{r}{R}\right)^2 + \text{const} \quad \text{for } -s \gg 1, \end{aligned}$$

or

$$\psi_0 = \text{const} \left(1 + \frac{1}{4}q \left(\frac{r}{R}\right)^2\right) \frac{r}{R} \quad \text{for } 0 < r \ll R.$$

Matching with (B 16), which we reformulate as

$$\psi_0 = \frac{\sqrt{2}}{q-1} \frac{1}{\left(\sqrt{2}\left(1 - \frac{r}{R}\right)\right)^{q-1}} \frac{1}{R^{q-1}} \quad \text{for } \frac{r}{R} \approx 1 \text{ with } 1 - \frac{r}{R} \gg \frac{1}{R}.$$

we deduce that

$$\psi_0 = C \left(1 + \frac{1}{4}q \left(\frac{r}{R}\right)^2\right) \frac{r}{R^q} \quad \text{for } 0 < r \ll R, \quad (\text{B } 17)$$

with C independent of R to leading order.

B.3.4 Scaling of (3.28)

In order to deduce the scaling (3.28), we collect the results (B 15), (B 16) and (B 17) just obtained in the case of $q > 1$:

$$\psi_0 = \left\{ \begin{array}{l} r - \left(1 - \frac{\sqrt{2}}{(q-1)R}\right) \frac{R^2}{r} \quad \text{for } r \geq R, \\ \frac{\sqrt{2}}{q-1} \frac{1}{(\sqrt{2}(R-r)+1)^{q-1}} \quad \text{for } r \approx R \text{ with } r \leq R, \\ C \left(1 + \frac{1}{4}q \left(\frac{r}{R}\right)^2\right) \frac{r}{R^q} \quad \text{for } 0 < r \ll R \end{array} \right\}. \quad (\text{B } 18)$$

We now see that for the integral under consideration, i.e.

$$-\int \psi_0 \partial_1 \bar{h} dx = -\pi \int_0^\infty \psi_0 \partial_r \bar{h} r dr \stackrel{(2.25)}{=} \frac{\sqrt{2}\pi}{R} \int_0^R \psi_0 r^2 dr,$$

there is a cross-over at $q = 2$: For $q < 2$, the cap region dominates, for $q > 2$, the foot region does. For $q < 2$ we infer the scaling $\frac{\sqrt{2}\pi}{R} \int_0^R \psi_0 r^2 dr \approx CR^{3-q}$ from the cap region behaviour in (B18). In case of $q \geq 2$, we conclude from the foot region behaviour in (B18):

$$\begin{aligned} \frac{\sqrt{2}\pi}{R} \int_0^R \psi_0 r^2 dr &\approx \frac{2\pi R}{q-1} \int_0^R \frac{1}{(\sqrt{2}(R-r)+1)^{q-1}} \left(\frac{r}{R}\right)^2 dr \\ &\approx \begin{cases} \sqrt{2}\pi R \ln R & \text{for } q = 2, \\ \frac{\sqrt{2}\pi R}{(q-2)(q-1)} & \text{for } q > 2 \end{cases}. \end{aligned}$$

This concludes showing (3.28) for $q > 1$.

B.4 Case $q = 1$: Recovering ψ_0 from u

We found in (B8), (B11) and (B12) that to leading order in $R \gg 1$:

$$u = \begin{cases} \frac{1}{\tanh\left(s + \frac{\ln(\sqrt{2}R)}{\sqrt{2}R}\right)} & \text{for } s > 0 \\ \frac{1}{\left(-s + \frac{1}{\sqrt{2}R}\right) \ln \frac{1}{-s + \frac{1}{\sqrt{2}R}}} & \text{for } 1 \gg -s > 0, \\ 1 + \frac{1}{2} \exp(2s) & \text{for } -s \gg 1, \end{cases} \quad (\text{B19})$$

B.4.1 Precursor region $s > 0$

As before, (3.23) translates into

$$\frac{d \ln \psi_0}{ds} = \frac{1 + \text{const} \exp(-2s)}{1 - \text{const} \exp(-2s)}.$$

To leading order in $R \gg 1$, (B19) behaves like

$$u \approx \frac{1 - \left(1 - 2 \frac{\ln(\sqrt{2}R)}{\sqrt{2}R}\right) \exp(-2s)}{1 + \left(1 - 2 \frac{\ln(\sqrt{2}R)}{\sqrt{2}R}\right) \exp(-2s)},$$

from which we obtain that $\text{const} = \left(1 - 2 \frac{\ln(\sqrt{2}R)}{\sqrt{2}R}\right)$ and therefore

$$\psi_0 = r - \left(1 - 2 \frac{\ln(\sqrt{2}R)}{\sqrt{2}R}\right) \frac{R^2}{r} \quad \text{for } r \geq R. \quad (\text{B20})$$

B.4.2 Foot region $0 < -s \ll 1$

From (B 19) we infer that

$$\ln \psi_0 = \ln \left(\ln \left(-s + \frac{1}{\sqrt{2R}} \right) \right) + \text{const}$$

and thus

$$\psi_0 = \text{const} \ln \left(1 - \frac{r}{R} + \frac{1}{\sqrt{2R}} \right) \quad \text{for } r \approx R \text{ with } r \leq R.$$

The matching with (B 20) yields

$$\psi_0 = -\sqrt{2} \ln \left(1 - \frac{r}{R} + \frac{1}{\sqrt{2R}} \right) \quad \text{for } r \approx R \text{ with } r \leq R. \quad (\text{B 21})$$

B.4.3 Cap region $-s \gg 1$

In the cap region we obtain as before

$$\psi_0 = \text{const} \left(1 + \frac{1}{4} \left(\frac{r}{R} \right)^2 \right) \frac{r}{R} \quad \text{for } 0 < r \ll R.$$

The constant is determined by matching with (B 21). Near the cap region, the term $1 - \frac{r}{R}$ dominates $\frac{1}{\sqrt{2R}}$ to leading order in $R \gg 1$, so that $\psi_0 \approx -\sqrt{2} \ln(1 - \frac{r}{R})$. The matching yields a constant $\text{const} = C_2$ which is independent of R . Hence

$$\psi_0 = C_2 \left(1 + \frac{1}{4} \left(\frac{r}{R} \right)^2 \right) \frac{r}{R} \quad \text{for } 0 < r \ll R.$$

Collecting the asymptotic expressions for ψ_0 in the different regions, we finally obtain

$$\psi_0 = \left\{ \begin{array}{l} r - \left(1 - 2 \frac{\ln(\sqrt{2R})}{\sqrt{2R}} \right) \frac{R^2}{r} \quad \text{for } r \geq R, \\ -\sqrt{2} \ln \left(1 - \frac{r}{R} + \frac{1}{\sqrt{2R}} \right) \quad \text{for } r \approx R \text{ with } r \leq R, \\ C_2 \left(1 + \frac{1}{4} \left(\frac{r}{R} \right)^2 \right) \frac{r}{R} \quad \text{for } 0 < r \ll R \end{array} \right\}. \quad (\text{B 22})$$

B.4.4 Scaling of (3.28)

As shown for $q < 1$, the contribution from the cap region to (3.28) is $\approx CR^2$ to leading order. The same holds for the foot region:

$$\frac{\sqrt{2}\pi}{R} \int_{\text{foot}} \psi_0 r^2 dr \stackrel{(\text{B 22})}{=} -\frac{2\pi}{R} \int_{\text{foot}} \ln \left(1 - \frac{r}{R} + \frac{1}{\sqrt{2R}} \right) r^2 dr \approx CR^2.$$

This proves (3.28) for $q = 1$.

B.5 Case $q < 1$: Recovering ψ_0 from u

We now turn to the case of $q < 1$ and recall that we argued that to leading order in $R \gg 1$:

$$u = \left\{ \begin{array}{ll} \frac{1}{\tanh\left(s + \frac{1}{C(\sqrt{2R})^q}\right)} & \text{for } s > 0 \\ \frac{C}{\left(-s + \frac{1}{\sqrt{2R}}\right)^q} & \text{for } 1 \gg -s > 0, \\ 1 + \frac{1}{2}q \exp(2s) & \text{for } -s \gg 1, \end{array} \right\}, \quad (\text{B 23})$$

where $C > 0$ denotes a constant independent of R .

B.5.1 Precursor region $s > 0$

With the same reasoning as before, this yields for the precursor region

$$\psi_0 = r - \left(1 - \frac{2}{C(\sqrt{2R})^q}\right) \frac{R^2}{r} \quad \text{for } r \geq R. \quad (\text{B 24})$$

B.5.2 Foot region $0 < -s \ll 1$

Now for the foot region. From (B 23) we infer that $\ln \psi_0$ must be of the form

$$\ln \psi_0 = -\frac{C}{q-1} \left(-s + \frac{1}{\sqrt{2R}}\right)^{1-q} + \text{const} \quad \text{for } 1 \gg -s > 0$$

and thus

$$\psi_0 = \text{const} \left(1 - \frac{C}{1-q} \left(1 - \frac{r}{R} + \frac{1}{\sqrt{2R}}\right)^{1-q}\right) \quad \text{for } r \approx R \text{ with } r \leq R.$$

The matching with (B 24) determines the multiplicative constant to leading order in $R \gg 1$:

$$\psi_0 = \frac{\sqrt{2}^{2-q} R^{1-q}}{C} - \frac{\sqrt{2}^{2-q} R^{1-q}}{1-q} \left(1 - \frac{r}{R} + \frac{1}{\sqrt{2R}}\right)^{1-q} \quad \text{for } r \approx R \text{ with } r \leq R. \quad (\text{B 25})$$

B.5.3 Cap region $-s \gg 1$

In the cap region we must have as before

$$\psi_0 = \text{const} \left(1 + \frac{1}{4}q \left(\frac{r}{R}\right)^2\right) \frac{r}{R} \quad \text{for } 0 < r \ll R.$$

Matching with (B 25), we gather that

$$\psi_0 = C_1 \left(1 + \frac{1}{4}q \left(\frac{r}{R}\right)^2\right) \frac{r}{R^q}$$

with a constant C_1 independent of R to leading order.

Collecting the asymptotic expressions for ψ_0 in the different regions, we finally obtain

$$\psi_0 = \left\{ \begin{array}{ll} r - \left(1 - \frac{2}{C(\sqrt{2}R)^q}\right) \frac{R^2}{r} & \text{for } r \geq R, \\ \sqrt{2}^{2-q} R^{1-q} \left(\frac{1}{C} - \frac{1}{1-q} \left(1 - \frac{r}{R} + \frac{1}{\sqrt{2}R}\right)^{1-q}\right) & \text{for } r \approx R \text{ with } r \leq R, \\ C_1 \left(1 + \frac{1}{4}q \left(\frac{r}{R}\right)^2\right) \frac{r}{R^q} & \text{for } 0 < r \ll R \end{array} \right\}. \quad (\text{B } 26)$$

B.5.4 Scaling of (3.28)

We infer the scaling of

$$- \int \psi_0 \partial_1 \bar{h} dx \stackrel{(2.25)}{=} \frac{\sqrt{2}\pi}{R} \int_0^R \psi_0 r^2 dr$$

from (B 26). Both the cap and the foot region reveal the scaling CR^{3-q} :

$$\frac{\sqrt{2}\pi}{R} \int_{\text{cap}} \psi_0 r^2 dr \stackrel{(\text{B } 26)}{=} \frac{\sqrt{2}\pi}{R} \int_{\text{cap}} C_1 \left(1 + \frac{1}{4}q \left(\frac{r}{R}\right)^2\right) \frac{r}{R^q} r^2 dr \approx CR^{3-q}$$

and

$$\begin{aligned} \frac{\sqrt{2}\pi}{R} \int_{\text{foot}} \psi_0 r^2 dr &\stackrel{(\text{B } 26)}{=} \sqrt{2}^{2-q} \pi R^{-q} \int_{\text{foot}} \left(\frac{1}{C} - \frac{1}{1-q} \left(1 - \frac{r}{R} + \frac{1}{\sqrt{2}R}\right)^{1-q}\right) r^2 dr \\ &\approx C(R^{3-q} + R). \end{aligned}$$

R^{3-q} dominates R , since $3 - q > 2$ for $q < 1$. This concludes the proof of (3.28) for $q < 1$.

Appendix C: Migration vs. sliding

It is enlightening to compare the problem of a near-equilibrium droplet migrating in a flux field prescribed at infinity to that of a near-equilibrium droplet sliding in an external potential field. The latter can be achieved physically, for example, by placing a droplet on an inclined surface where gravity plays the role of the field [16, 18]. In reference [15, III.C], it was envisioned that this is the same as migration in a prescribed flux field. However, as we shall discuss towards the end of this subsection, our findings deviate from theirs. In analogy to a constant flux field f_∞ at infinity we consider an external potential with constant gradient:

$$\mu_{\text{ext}} = -f_\infty \cdot (x - X). \quad (\text{C } 1)$$

We argue that the drift velocity \dot{X} of the droplet is determined by the following problem:

$$-\dot{X} \cdot \nabla \bar{h} - \nabla \cdot (\bar{m} \nabla \mu) = 0, \quad (\text{C2})$$

$$J \cdot \nu \rightarrow 0 \quad \text{as } r \uparrow \infty \quad \text{where } J := -\bar{m} \nabla \mu, \quad (\text{C3})$$

$$\int \mu \nabla \bar{h} dx = f_\infty \int (\bar{h} - \bar{h}_\infty) dx. \quad (\text{C4})$$

Analogous to Subsection 3.1, we can give two arguments in favour of this, either based on the Rayleigh principle or based on a solvability argument. For shortness, we skip this part.

As before, we seek a better characterization of the \dot{X} - f_∞ -relationship implicitly defined by (C2), (C3) and (C4). Again, in the case of a 1- d substrate, we obtain a fairly explicit expression: From (3.7) and the no-flux boundary condition of J we infer $J = \dot{X}(\bar{h} - \bar{h}_\infty)$ and thus obtain from the variation w.r.t. \dot{X} in the Rayleigh principle argument

$$0 = \int (\bar{h} - \bar{h}_\infty) \left(\frac{1}{\bar{m}} \dot{X} (\bar{h} - \bar{h}_\infty) - f_\infty \right) dx$$

or

$$\dot{X} = \frac{\int (\bar{h} - \bar{h}_\infty) dx}{\int \frac{1}{\bar{m}} (\bar{h} - \bar{h}_\infty)^2 dx} f_\infty. \quad (\text{C5})$$

Notice that formula (C5) differs from (D1) not just by the sign (droplets drift *in* direction of the force f_∞ coming from the external potential) but in structure. Since $\bar{m} \gg 1$ in the droplets, the reaction to J_∞ is much weaker than to f_∞ .

The formula for a 2- d substrate relates to (C5) as (3.18) does to (D1):

$$\dot{X} = \frac{\int (\bar{h} - \bar{h}_\infty) dx}{\int \psi_1 \partial_1 \bar{h} dx} f_\infty.$$

Indeed, this identity follows from (C4) since $\mu = \dot{X} \psi_1$. As before, (3.17) and integration by parts of the denominator yield

$$\dot{X} = \frac{\int (\bar{h} - \bar{h}_\infty) dx}{\int \bar{m} |\nabla \psi_1|^2 dx} f_\infty. \quad (\text{C6})$$

Notice that (3.24) and (C6) have the same denominator. The authors of [15] call this quantity, which we shall analyse more closely in Section A, ‘dissipative integral’ – rightfully so, since in view of (3.17) it is the rate of energy dissipation when an equilibrium droplet moves with unit speed in an environment quiescent far away from the droplet. However, our formula

$$I := \int \bar{m} |\nabla \psi_1|^2 dx \quad (\text{C7})$$

is not quite the same as theirs:

$$I := \int \frac{1}{\bar{m}} \bar{h} (\bar{h} - \bar{h}_\infty) dx, \quad (\text{C8})$$

cf. [15, formula (14)]. Formula (C 8) has the same flavour as the one-dimensional expression $\int \frac{1}{\bar{m}} (\bar{h} - \bar{h}_\infty)^2 dx$ (cf. (C 5)). This difference stems from ignoring divergence-free fields when integrating the thin-film equation to obtain equation [15, formula (9)] in their work. In particular, the flux that we find, $-m\nabla\psi_1$, is dipolar (3.20), while the flux, j , of Pismen and Pomeau is unidirectional. Also if the flux is assumed to tend towards zero as $|x| \rightarrow \infty$, then the r.h.s. of [15, formula (9)] should read (in our notation) $C(h - h_\infty)/\bar{m}$ instead of Ch/\bar{m} . We see in Subsection A.3 (in particular in (A 14) and (A 15)) that for sufficiently monotone mobilities in the sense of $q \geq 3$, the two expressions, (C 7) and $\int \frac{1}{\bar{m}} (\bar{h} - \bar{h}_\infty)^2 dx$, differ only by a factor of 2 in the regime of large equilibrium droplets. The factor 2 is due to the dipolar nature of the flux; it enters (A 9) as the consequence of $\frac{1}{2\pi} \int_0^{2\pi} \cos^2 \varphi d\varphi = \frac{1}{2}$.

Appendix D: Analysis in one-dimensional setting

D.1 Characterization and sign of the migration velocity

The continuity equation (3.7) combined with the flux boundary conditions (3.2) implies

$$J = J_\infty + \dot{X} (\bar{h} - \bar{h}_\infty).$$

Inserting this identity into (3.8) yields

$$0 = J_\infty \int \frac{1}{\bar{m}} (\bar{h} - \bar{h}_\infty) dx + \dot{X} \int \frac{1}{\bar{m}} (\bar{h} - \bar{h}_\infty)^2 dx,$$

or

$$\dot{X} = - \frac{\int \frac{1}{\bar{m}} (\bar{h} - \bar{h}_\infty) dx}{\int \frac{1}{\bar{m}} (\bar{h} - \bar{h}_\infty)^2 dx} J_\infty, \quad (\text{D } 1)$$

which is identical with the formula derived in [8, formula (4.10)] by the above solvability argument. In particular, the droplet migrates in the direction *opposite* to the prescribed flux. If the flux goes from left to right, one should think of the droplet gaining mass at its left end while losing mass at its right end, thus drifting to the left.

D.1.1 Scaling of migration velocity

One has to investigate integrals of the form

$$I_\gamma := \int \frac{1}{\bar{m}} (\bar{h} - \bar{h}_\infty)^\gamma dx = \int \frac{(\bar{h} - \bar{h}_\infty)^\gamma}{\bar{h}^q} dx.$$

Obviously, there is a cross-over at $q = \gamma + 1$: For $q < \gamma + 1$, the contribution from the cap region dominates I_γ , while for $q > \gamma + 1$, the contribution from the foot region dominates.

We appeal to the first integral of $-\partial_x^2 \bar{h} + U'(\bar{h}) = P$, that is,

$$-\frac{1}{2} (\partial_x \bar{h})^2 + W(\bar{h}) = 0, \quad (\text{D } 2)$$

where W is defined in (2.7). Because of (2.4) (which *a fortiori* holds in the one-dimensional case), (D 2) turns into

$$\partial_x \bar{h} = -\sqrt{2W(\bar{h})} \quad \text{for } x > 0,$$

so that

$$I_\gamma = 2 \int_{\bar{h}_\infty}^{\bar{h}(x=0)} \frac{(h - \bar{h}_\infty)^\gamma}{h^q} \frac{1}{\sqrt{2W(h)}} dh. \quad (\text{D } 3)$$

Recall that $\bar{h}_\infty \rightarrow 1$ as $P \downarrow 0$ (cf. (2.2)) so that to leading order, (D 3) turns into

$$\begin{aligned} I_\gamma &\approx 2 \int_1^{\bar{h}_{\text{meso}}(0)} \frac{(h-1)^\gamma}{h^q} \frac{1}{\sqrt{2U(h)}} dh \\ &\stackrel{(2.25)}{=} 2 \int_1^{1+R/\sqrt{2}} \frac{(h-1)^\gamma}{h^q} \frac{1}{\sqrt{2U(h)}} dh, \end{aligned} \quad (\text{D } 4)$$

since due to $\gamma > 0$, the (potential) singularity at $h = 1$ is integrable.

For $q > \gamma + 1$, (D 4) is also integrable at $h \uparrow \infty$, so that to leading order I_γ is independent of R :

$$I_\gamma \approx 2 \int_1^\infty \frac{(h-1)^\gamma}{h^q} \frac{1}{\sqrt{2U(h)}} dh \in (0, \infty).$$

Note that the leading order scaling of I_γ depends on the details of the potential U .

On the other hand, for $q = \gamma + 1$, we have a logarithmic divergence

$$I_\gamma \approx \sqrt{2} \ln R,$$

and for $q < \gamma + 1$, the divergence

$$I_\gamma \approx CR^{\gamma-q+1}.$$

Thus in case of a one-dimensional substrate, we find the following scaling to leading order in $R \gg 1$:

$$\int \frac{1}{\bar{m}} (\bar{h} - \bar{h}_\infty)^2 dx = \begin{cases} CR^{3-q} & \text{for } q \in [0, 3), \\ \sqrt{2} \ln R & \text{for } q = 3, \\ C & \text{for } q > 3 \end{cases} \quad (\text{D } 5)$$

$$\int \frac{1}{\bar{m}} (\bar{h} - \bar{h}_\infty) dx = \begin{cases} CR^{2-q} & \text{for } q \in [0, 2), \\ \sqrt{2} \ln R & \text{for } q = 2, \\ C & \text{for } q > 2 \end{cases} \quad (\text{D } 6)$$

where $C > 0$ denotes a generic constant independent of R (but dependent on q).

D.2 Interacting mesoscopic droplets: Two droplet case

We now carry out the analysis of Section 4 for the one-dimensional setting. Let us first consider a configuration of two droplets (see Figure D 1) where we set $L := L_{12}$. The

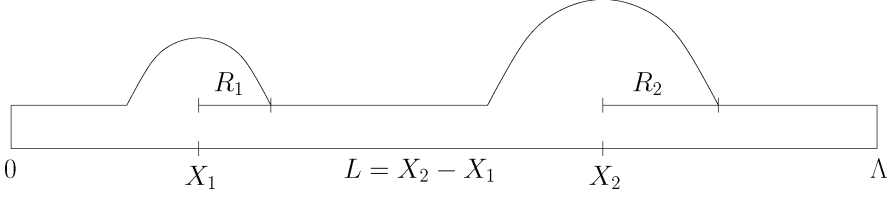


FIGURE D 1. Droplet configuration.

change vectors have the form $v = (\dot{V}_1, -\dot{V}_1, \dot{X}_1, \dot{X}_2)^T \in \mathbb{R}^4$ or, in Eulerian coordinates,

$$\Delta h_v = -\partial_x h_1(x) \dot{X}_1 - \partial_x h_2(x) \dot{X}_2 + \left(\frac{\partial h_1}{\partial V_1} - \frac{\partial h_2}{\partial V_2} \right) \dot{V}_1.$$

The matrix G representing the dissipation rate is a matrix in $\mathbb{R}^{4 \times 4}$ with sub-matrices G^v , G^m and C in $\mathbb{R}^{2 \times 2}$, as in (4.14).

We determine the approximate values of coefficients in the regime (4.1) of large, far apart droplets.

Computing G^v

Let $w := (1, -1, 0, 0)^T$. Then $-\partial_x J_w = \Delta h_w = \frac{\partial h_1}{\partial V_1} - \frac{\partial h_2}{\partial V_2}$. Hence

$$\begin{aligned} w^T G w &= G_{11}^v - G_{12}^v - G_{21}^v + G_{22}^v \\ &= \int \frac{1}{m(h(x))} |J_w(x)|^2 dx \end{aligned}$$

The above is the only requirement on coefficients of G^v , which allows us to define

$$\begin{aligned} G_{11}^v &= G_{22}^v := 0 \\ G_{12}^v &= G_{21}^v := -\frac{1}{2} \int \frac{1}{m(h(x))} |J_w|^2 dx. \end{aligned}$$

Elementary integration yields

$$J_w(x) = \begin{cases} 0 & \text{outside,} \\ -\frac{1}{6\sqrt{2\omega}} V_1^{-\frac{3}{2}} (x - X_1)^3 - \frac{1}{4\sqrt{2\omega}} V_1^{-\frac{1}{2}} (x - X_1) - \frac{1}{2} & \text{in } B(X_1, R_1), \\ -1 & \text{in between,} \\ \frac{1}{6\sqrt{2\omega}} V_2^{-\frac{3}{2}} (x - X_2)^3 + \frac{1}{4\sqrt{2\omega}} V_2^{-\frac{1}{2}} (x - X_2) - \frac{1}{2} & \text{in } B(X_2, R_2), \\ 0 & \text{outside.} \end{cases}$$

In the regime $L \gg R_i$, the dissipation tensor is to the leading order

$$\int \frac{1}{m} |J_w|^2 dx = \int_{B(X_1, R_1)} \frac{1}{m} |J_w|^2 dx + \underbrace{\int_{X_1+R_1}^{X_2-R_2} 1 dx}_{\approx L} + \int_{B(X_2, R_2)} \frac{1}{m} |J_w|^2 dx \approx L,$$

since the two integrals over $B(X_i, R_i)$ scale like R_i . In conclusion

$$G_{ii}^v = 0 \quad (\text{D } 7a)$$

$$G_{12}^v = G_{21}^v \approx -\frac{1}{2}L. \quad (\text{D } 7b)$$

Computing G^m

Let $w_1 := (0, 0, 1, 0)^T$ and $w_2 := (0, 0, 0, 1)^T$. Then $-\partial_x J_{w_i} = \Delta h_{w_i} = -\partial_x h_i$, for $i = 1, 2$. Hence

$$G_{ii}^m = w_i^T G w_i = \int \frac{1}{m(h(x))} |J_{w_i}(x)|^2 dx.$$

Elementary integration yields $J_{w_i}(x) = h_i(x)$ and thus

$$G_{ii}^m = \int \frac{1}{m(h(x))} (h_i(x))^2 dx =: g_i. \quad (\text{D } 8a)$$

Since J_{w_i} has support in $B(X_i, R_i)$, it follows that

$$G_{12}^m = G_{21}^m = \int \frac{1}{m(h(x))} J_{w_1}(x) \cdot J_{w_2}(x) dx = 0. \quad (\text{D } 8b)$$

Computing C

For $i = 1, 2$

$$\begin{aligned} w_i^T G w &= C_{i1} - C_{i2} \\ &= \int \frac{1}{m(h(x))} J_{w_i}(x) \cdot J_w(x) dx, \quad \text{where } \begin{aligned} -\partial_x J_{w_i} &= -\partial_x h_i \\ -\partial_x J_w &= \frac{\partial h_1}{\partial V_1} - \frac{\partial h_2}{\partial V_2} \end{aligned} \\ &= \int_{B(X_i, R_i)} \frac{1}{m(h(x))} h_i(x) (c(x - X_i)^3 + \check{c}(x - X_i) - \frac{1}{2}) dx \\ &= -\frac{1}{2} \int_{B(X_i, R_i)} \frac{1}{m(h(x))} h_i(x) dx. \end{aligned}$$

This allows us to define

$$C_{11} = C_{22} = 0, \quad (\text{D } 9a)$$

$$C_{12} = c_1 := \frac{1}{2} \int_{B(X_1, R_1)} \frac{1}{m(h(x))} h_1(x) dx, \quad (\text{D } 9b)$$

$$C_{21} = -c_2 := -\frac{1}{2} \int_{B(X_2, R_2)} \frac{1}{m(h(x))} h_2(x) dx. \quad (\text{D } 9c)$$

Collecting the results of (D 8), (D 7) and (D 9), the full matrix G is given by

$$G = \begin{bmatrix} 0 & -\frac{1}{2}L & 0 & -\frac{1}{2} \int \frac{1}{m} h_2 dx \\ -\frac{1}{2}L & 0 & \frac{1}{2} \int \frac{1}{m} h_1 dx & 0 \\ 0 & \frac{1}{2} \int \frac{1}{m} h_1 dx & \int \frac{1}{m} h_1^2 dx & 0 \\ -\frac{1}{2} \int \frac{1}{m} h_2 dx & 0 & 0 & \int \frac{1}{m} h_2^2 dx \end{bmatrix} \quad (\text{D } 10)$$

to the leading order.

Rayleigh dynamics

Note that $\nabla E = \frac{\sqrt{2}}{\omega} (V_1^{-\frac{1}{2}}, V_2^{-\frac{1}{2}}, 0, 0)^T$. According to (4.13), coordinates of $\hat{\Theta} = (\dot{V}_1, \dot{V}_2, \dot{X}_1, \dot{X}_2)^T$ are the solutions of the following system of linear ODEs:

$$\begin{aligned} \dot{V}_1 + \dot{V}_2 &= 0, \\ G_{12}^v(\dot{V}_2 - \dot{V}_1) - c_2 \dot{X}_2 - c_1 \dot{X}_1 &= -\frac{\sqrt{2}}{\omega} (V_1^{-\frac{1}{2}} - V_2^{-\frac{1}{2}}), \\ c_1 \dot{V}_2 + g_1 \dot{X}_1 &= 0, \\ -c_2 \dot{V}_1 + g_2 \dot{X}_2 &= 0. \end{aligned}$$

Solving the system yields for the volume change

$$\dot{V}_1 = \frac{\sqrt{2}}{\omega} \left(\frac{c_1^2}{g_1} + \frac{c_2^2}{g_2} + 2G_{12}^v \right)^{-1} (V_1^{-\frac{1}{2}} - V_2^{-\frac{1}{2}}),$$

and for the migration

$$\dot{X}_1 = \frac{\sqrt{2}}{\omega} \frac{c_1}{g_1} \left(\frac{c_1^2}{g_1} + \frac{c_2^2}{g_2} + 2G_{12}^v \right)^{-1} (V_1^{-\frac{1}{2}} - V_2^{-\frac{1}{2}}).$$

Note that in the regime $L \gg V_i^{\frac{1}{2}}$, using the estimates on the coefficients from (D 5) and (D 6) we obtain $G_{12}^v \gg \frac{c_1^2}{g_1} + \frac{c_2^2}{g_2}$, so that

$$\left(\frac{c_1^2}{g_1} + \frac{c_2^2}{g_2} + 2G_{12}^v \right) \approx 2G_{12}^v \approx -L.$$

Therefore

$$\dot{V}_1 = \frac{\sqrt{2}}{\omega} \frac{1}{L} (V_2^{-\frac{1}{2}} - V_1^{-\frac{1}{2}}), \quad (\text{D } 11)$$

$$\dot{X}_1 = \frac{\sqrt{2}}{\omega} \frac{1}{L} \frac{\int \frac{1}{m(h)} h_1 dx}{\int \frac{1}{m(h)} h_1^2 dx} (V_2^{-\frac{1}{2}} - V_1^{-\frac{1}{2}}). \quad (\text{D } 12)$$

D.3 Interacting mesoscopic droplets: n -droplet case

The computation of the matrix G in $\mathbb{R}^{2n \times 2n}$ is analogous to the two-droplet case. In particular,

$$\begin{aligned} G_{ij}^v &= -\frac{1}{2}L_{ij}, \\ C &= \text{diag}(c_1, \dots, c_n) T, \quad \text{where } T_{ij} := \begin{cases} 1 & \text{if } i < j, \\ 0 & \text{if } i = j, \\ -1 & \text{if } i > j, \end{cases} \\ G^m &= \text{diag}(g_1, \dots, g_n). \end{aligned} \tag{D 13}$$

It is easy to check that the choice $G_{ij}^v = -\frac{1}{2}L_{ij}$ is consistent with (D 7).

To determine the dynamics in a transparent form, assume that $X_i < X_{i+1}$ for all $i = 1, \dots, n-1$. Let us use the notation $\dot{V} = (\dot{V}_1, \dots, \dot{V}_n)^T$ and $\dot{X} = (\dot{X}_1, \dots, \dot{X}_n)^T$. The equations of the dynamics are then

$$\begin{aligned} (I - pp^T)(G^v \dot{V} + C^T \dot{X}) &= -(I - pp^T)\nabla_V E \\ C \dot{V} + G^m \dot{X} &= 0. \end{aligned}$$

Here, p has been restricted to its first n coordinates. It follows that

$$\dot{X} = -\text{diag}\left(\frac{c_1}{g_1}, \dots, \frac{c_n}{g_n}\right) T \dot{V}. \tag{D 14}$$

Substituting in the first equation and observing that, as for two droplets,

$$C(G^m)^{-1}C^T \ll G^v$$

gives the following approximation when $L_{ij} \gg V_k^{\frac{1}{2}} \gg 1$ for $i, j, k = 1, \dots, n, i \neq j$:

$$(I - pp^T)G^v \dot{V} = -(I - pp^T)\nabla_V E. \tag{D 15}$$

The remainder of this subsection is devoted to finding a solution of this equation with $\sum_i \dot{V}_i = 0$. For this purpose, note that the sub-matrix G^v has the form of a Green's function in one dimension: The i -th entry of the product $G^v \dot{V}$, i.e.

$$-\frac{1}{2} \sum_{j \neq i} |X_i - X_j| \dot{V}_j,$$

realizes the superposition of potentials in X_i generated by 'mass sources' at X_j with masses \dot{V}_j . Thus, it is reasonable that equation (D 15) can be solved by applying a discrete Laplace operator D that has the form of a tri-diagonal matrix:

$$D_{ij} := \begin{cases} \frac{1}{L_{i-1i}} & \text{if } j = i - 1 \\ -\left(\frac{1}{L_{i-1i}} + \frac{1}{L_{i+1i}}\right) & \text{if } j = i \\ \frac{1}{L_{i+1i}} & \text{if } j = i + 1 \\ 0 & \text{else,} \end{cases}$$

with no-flux condition at the boundary. We used the convention $L_{01} = \infty$ $L_{nn+1} = \infty$. Note that $D(I - pp^T) = D$.

Indeed, a direct calculation of $-DG^v$ based on the relation $L_{ij+1} = L_{ij} + L_{j+1}$ yields

$$-DG^v = \frac{1}{2} \begin{pmatrix} 1 & -1 & \dots & \dots & -1 \\ & 2 & & & \\ & & \ddots & & \\ & & & 2 & \\ -1 & \dots & \dots & -1 & 1 \end{pmatrix},$$

and finally, using the conservation of volume $\sum_i \dot{V}_i = 0$, the identity

$$-DG^v \dot{V} = \dot{V}.$$

Applying the same transformation to the r.h.s. gives for $i = 1, \dots, n$

$$\frac{(\nabla E)_{i+1} - (\nabla E)_i}{L_{i+1}} - \frac{(\nabla E)_i - (\nabla E)_{i-1}}{L_{i-1}} = \frac{\sqrt{2}}{\omega} \left(\frac{V_{i+1}^{-\frac{1}{2}} - V_i^{-\frac{1}{2}}}{L_{i+1}} - \frac{V_i^{-\frac{1}{2}} - V_{i-1}^{-\frac{1}{2}}}{L_{i-1}} \right),$$

where we let $L_{01} = L_{nn+1} = \infty$. Hence, we obtain the equation for the volume change given by (D 15):

$$\dot{V}_i = \frac{\sqrt{2}}{\omega} \left(\frac{V_{i+1}^{-\frac{1}{2}} - V_i^{-\frac{1}{2}}}{L_{i+1}} - \frac{V_i^{-\frac{1}{2}} - V_{i-1}^{-\frac{1}{2}}}{L_{i-1}} \right). \quad (\text{D } 16)$$

To determine \dot{X} , we use (D 14). It follows from (D 16) that

$$\dot{X}_i = \frac{\sqrt{2}}{\omega} \frac{\int \frac{1}{m(h)} h_i dx}{\int \frac{1}{m(h)} h_i^2 dx} \left(\frac{V_i^{-\frac{1}{2}} - V_{i-1}^{-\frac{1}{2}}}{L_{i-1}} + \frac{V_{i+1}^{-\frac{1}{2}} - V_i^{-\frac{1}{2}}}{L_{i+1}} \right). \quad (\text{D } 17)$$

Now it is easy to check that equations (D 16) and (D 17) indeed coincide with the equations of motion and pressure change proposed by Glasner and Witelski in [8]. To switch between the volume and the pressure one applies the relation $P_i = \frac{\sqrt{2}}{\omega} V_i^{-\frac{1}{2}}$.

D.4 Time scales of the dynamics

From (D 11) and (D 12), we can deduce heuristically the typical time scales for Ostwald ripening and migration for a configuration of many droplets. We recall the assumption $L \gg V^{\frac{1}{2}}$.

Ostwald ripening

From (D 11) we obtain

$$\dot{V} \sim \frac{1}{L} V^{-\frac{1}{2}}.$$

Hence the time scale for ripening is

$$\tau_{\text{rip}} \sim \frac{V}{\bar{V}} \sim LV^{\frac{3}{2}} \sim V^{\frac{5}{2}}/\bar{H}. \quad (\text{D } 18)$$

Here we used mass conservation (4.27).

Migration

Equation (D 12) implies the scaling

$$\dot{L} \sim |\dot{X}| \sim \frac{c}{g} \frac{1}{L} V^{-\frac{1}{2}}$$

and therefore

$$\tau_{\text{mig}} \sim \frac{L}{\dot{L}} \sim \frac{g}{c} L^2 V^{-\frac{1}{2}} \sim \frac{g}{c} V^{\frac{3}{2}}/\bar{H}^2.$$

Here, g and c denote the coefficients of the migration and the coupling matrix, respectively, for a typical droplet. From (D 5) and (D 6) we deduce the scaling

$$\frac{c}{g} = \frac{1}{2} \frac{\int_{B(X,R)} \frac{1}{m} h dx}{\int_{B(X,R)} \frac{1}{m} (h)^2 dx} \sim \begin{cases} V^{-\frac{1}{2}} & q \in [0, 2), \\ V^{-\frac{1}{2}} \ln V & q = 2, \\ V^{\frac{q-3}{2}} & q \in (2, 3), \\ \ln^{-1} V & q = 3, \\ 1 & q > 3. \end{cases} \quad (\text{D } 19)$$

Hence the time scale for the droplet migration is

$$\tau_{\text{mig}} \sim \frac{V^{\frac{5}{2}}}{\bar{H}^2} \begin{cases} V^{\frac{1}{2}} & q \in [0, 2), \\ V^{\frac{1}{2}} \ln^{-1} V & q = 2, \\ V^{\frac{3-q}{2}} & q \in (2, 3), \\ \ln V & q = 3, \\ 1 & q > 3. \end{cases} \quad (\text{D } 20)$$

The relative importance of migration depending on V and \bar{H} can be deduced from the quotient of the time scales:

$$\frac{\tau_{\text{rip}}}{\tau_{\text{mig}}} \sim \bar{H} \begin{cases} V^{-\frac{1}{2}} & q \in [0, 2), \\ V^{-\frac{1}{2}} \ln V & q = 2, \\ V^{\frac{q-3}{2}} & q \in (2, 3), \\ \ln^{-1} V & q = 3, \\ 1 & q > 3. \end{cases}$$

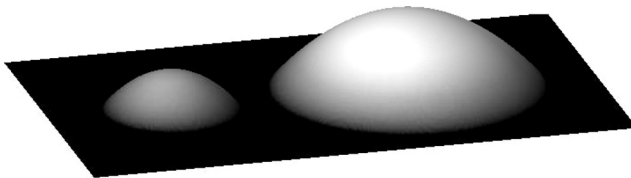


FIGURE E 1. Initial configuration of two droplets on a domain with Neumann boundary conditions.

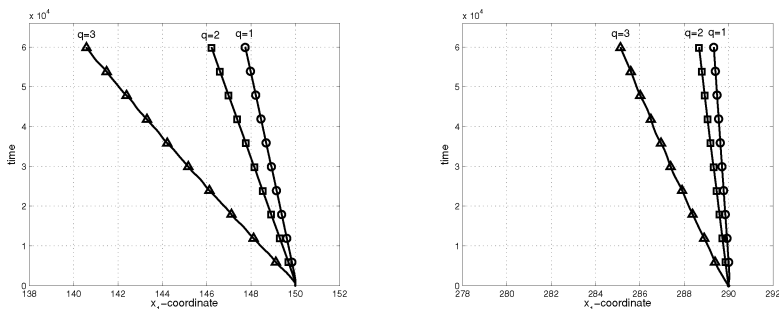


FIGURE E 2. Trajectories of x_1 -components of the centers X_1 (left) and X_2 (right).

Appendix E: Numerical simulations

E.1 Dependence on mobility

The propensity of a droplet to migrate on the precursor layer strongly depends on the mobility exponent q . Based on the discretization of the full PDE (1.9) introduced in [13] with Neumann boundary conditions, we choose the following set-up for a numerical test (see Figure E 1):

- domain $[0, L_x] \times [0, L_y]$, where $L_x = 300$ and $L_y = 150$, and
- an initial configuration of two droplets with radii $R_1(0) = 20$ and $R_2(0) = 40$ and centers at $X_1(0) = (120, 75)^T$ and $X_2(0) = (200, 75)^T$.

We compare the migration of the droplets for three different (physically relevant) mobilities: $q = 1, 2, 3$. The positions only change in the first coordinate, so that it is sufficient to monitor the x_1 -coordinates X_1^1 and X_2^1 of the centers (see Figure E 2). A qualitative comparison of the different mobilities reveals

- that the migration velocity increases with q , and
- that the smaller droplet is faster than the bigger one

in accordance with the scaling relations in (4.29).

E.2 Collision vs. collapse

From the scaling relations (4.30) we infer that the time scales for Ostwald ripening and migration are comparable (up to a logarithm) in the case of $q = 3$. These relations are

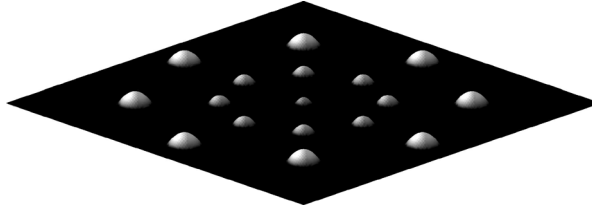


FIGURE E 3. Initial configuration for the numerical simulation of the reduced ODE system.

based on the reduced system of ODEs (4.13) with coefficients (4.2.1) derived by asymptotic analysis in the regime $1 \ll R \ll L$.

We conducted numerical tests solving the system of ODEs to show that migration indeed can play a role in the coarsening process – depending on the mobility exponent. Let us mention that an explicit knowledge of the constants in the asymptotic expressions (4.20) and (4.21) is necessary for the simulations.

Large time horizons are needed in the test runs: The bigger the typical distance between droplets, the slower the volume change and the migration speed. On the other hand, the vanishing of a droplet happens on a much faster time scale. Hence we use an adaptive time stepping controlled by the smallest droplet volume of the configuration.

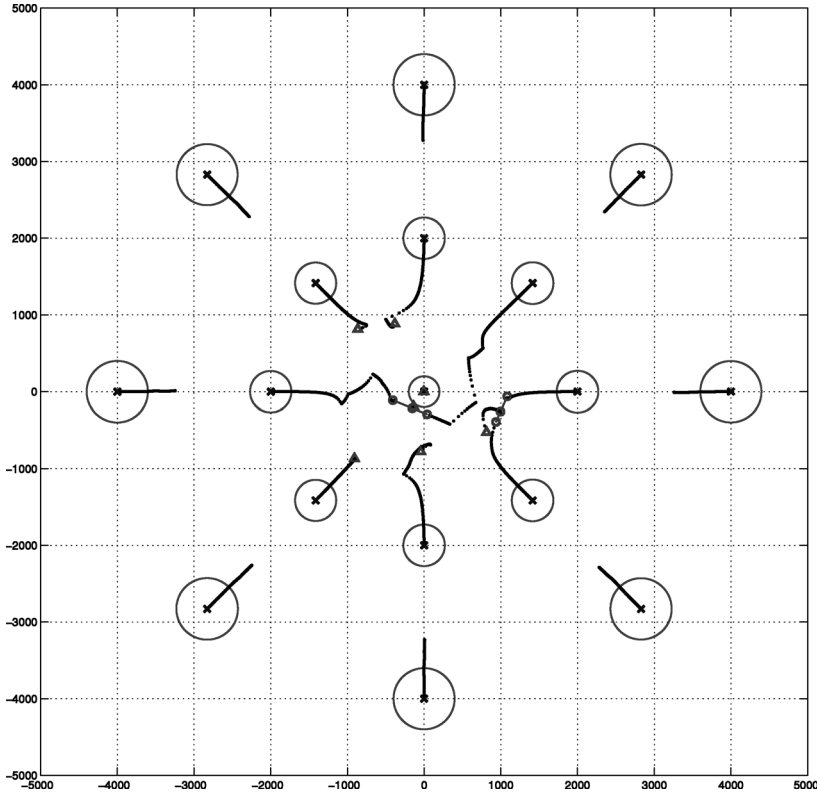
As an initial configuration we consider two rings of each eight droplets and one center droplet (see Figure E 3). The typical radius of the droplets in the outer ring is ≈ 400 but randomly perturbed in the range of 1%, in the inner ring ≈ 250 (again randomly perturbed); the center droplet has radius 200. The droplet distances vary between 1600 and 2000.

The subsequent figures show the trajectories of the centers over the total time $T = 10^{10}$ derived from the reduced system of ODEs for mobility exponents $q = 2$ and $q = 3$. We take exactly the same initial configuration for both exponents. Let us first give some explanations:

- The crosses are the initial positions of the droplets. The grey circles give the initial size.
- When a droplet vanishes, its last position is given by a triangle.
- In case of a droplet collision, the centers of the two involved droplets marked by circles are merged along the line to a new one (also depicted by a circle).

Let us first consider the case $q = 3$ in Figures E 4 and E 5:

- Since the average radius of a droplet in the outer ring is much larger than in the inner ring, all droplets migrate towards the center droplet positioned at the origin. The center droplet vanishes first.
- Every change in the number of droplets affects the movement of the remaining droplets immediately; the trajectories are non-smooth. So each singularity of a trajectory can be related to a disappearance of a droplet.
- In Figure E 5 one can inspect two collision events along the red lines. The asymmetric coalescence is due to the different droplet sizes (see the comment on the ‘merging rule’ below).

FIGURE E4. Trajectories in the case $q = 3$.

- The varying resolution of the trajectories reveals that the migration speed of each droplet varies: The closer a droplet is to another one, the faster they both move.
- Eventually all droplets in the inner ring vanish (including the newly merged ones), only the outer ring of larger droplets survives.
- The total balance of the evolution is: two collisions and seven collapses.

A ‘merging rule’ for two droplets in the one-dimensional case is proposed in [9]. We adapt it analogously for the two-dimensional case: Due to mass conservation the volume of the merged droplet is the sum of the volumes of the collided droplets. Its position is symmetric with respect to the outer contact lines of the two droplets along the difference vector $X_2^{\text{old}} - X_1^{\text{old}}$, that is

$$X^{\text{new}} = \frac{1}{2}(X_1^{\text{old}} + X_2^{\text{old}}) + \frac{1}{2L}(R_2^{\text{old}} - R_1^{\text{old}})(X_2^{\text{old}} - X_1^{\text{old}}).$$

Let us clearly state that in the two-dimensional case no analysis has been done for a further justification of this rule.

In the case of $q = 2$ (see Figure E 6) collisions do not occur; the dominating coarsening process is Ostwald ripening. Furthermore, the droplets migrate much slower as can be seen from the lengths of the trajectories.

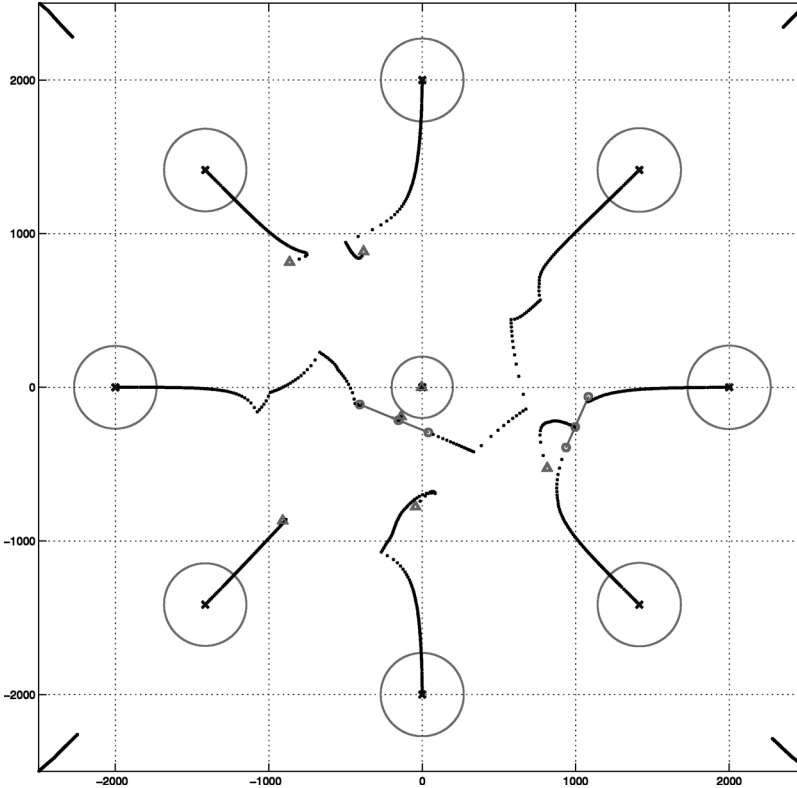


FIGURE E 5. A closer look at collisions in the case $q = 3$.

Appendix F: Relationship to matched asymptotic expansions

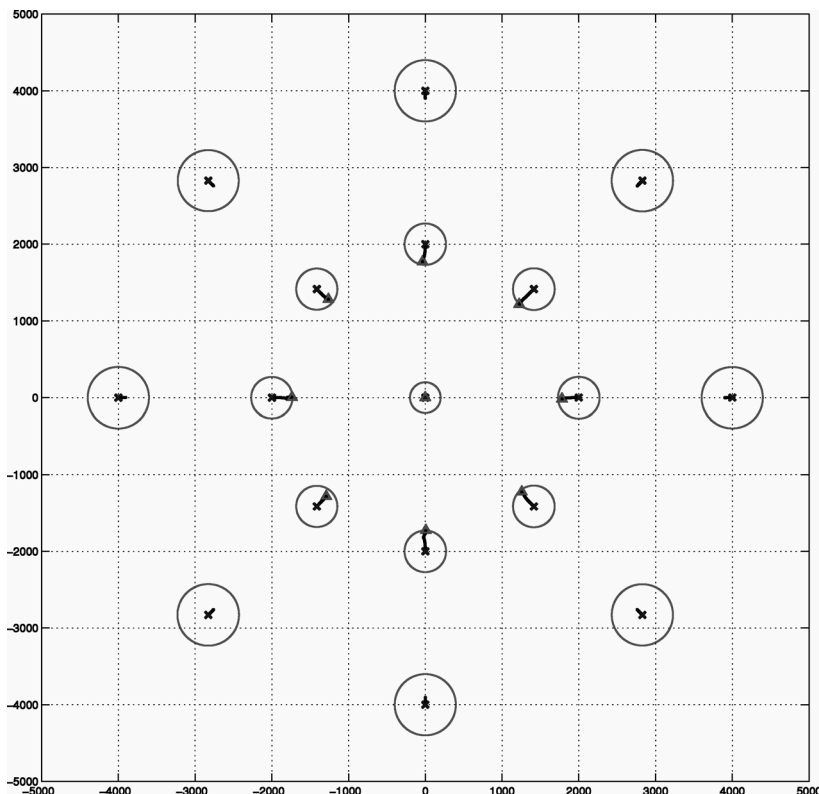
Much of the foregoing analysis can also be phrased in the language of matched asymptotic expansions [7]. Here we briefly summarize the connections between the current presentation and this alternative approach.

The asymptotic droplet profiles (2.22–2.24) and other approximations were derived under the assumption of large droplet size $R \rightarrow \infty$ compared to a fixed precursor thickness. One could alternatively rescale the thin-film equation as

$$x' = x/R_0, \quad h' = h/R_0, \quad (\text{F } 1)$$

where R_0 is a typical droplet radius. Under this rescaling, droplets have the same contact angle, but their size is of order unity. The precursor film layer has thickness $1/R_0 \equiv \varepsilon \ll 1$, and the width of the foot region under such a rescaling is also of order ε . This suggests the use of matched asymptotic expansions in three regions:

- *Precursor region*: The solution is expanded as $h = \varepsilon h_1 + \varepsilon^2 h_2 + \dots$. The correction term h_2 satisfies the exterior Laplace equation that describes quasi-stationary diffusion, whose boundary conditions are given by matching across the foot layers of each droplet. The flux which droplets experience arises at this level in the same fashion as flux arises in the Mullins–Sekerka reduction of the Cahn–Hilliard equation [14].

FIGURE E.6. Trajectories in the case $q = 2$.

- *Foot region*: The solution has the expansion $h = \varepsilon H_1(z) + \varepsilon^2 H_2(z) + \dots$ where $z = (R(t) - r)/\varepsilon$ is a stretched radial coordinate. The leading order solution recovers the foot region solution given implicitly in equation (2.15).
- *Cap region*: The solution has the expansion $h = h_0 + \varepsilon^\alpha h_1 + \dots$. At leading order one recovers the parabolic cap solution (2.22–2.24). The exponent α depends on q and is determined by matching requirements.

The expansions in the foot and cap region are carried to further orders whose scaling in ε is prescribed by the mobility exponent q . These choices ultimately lead to matching conditions between the foot and cap layers, and suggest how time should scale as a function of ε . The cases $q = 2, 3$ are, of course, somewhat delicate because they lead to logarithmic terms in the expansions.

In the cap and foot regions, the correction terms (call them h_1) satisfy a linear equation of the form

$$MLh_1 = f, \quad \text{where} \quad M\mu = -\nabla \cdot (\bar{m}\nabla\mu) \quad \text{and} \quad Lh' = -\Delta h_1 + U''(h_0)h_1. \quad (\text{F } 2)$$

Fredholm-type solvability conditions are derived from (null) eigenfunctions ψ of the

adjoint problem, which can be written as

$$Lh'_0 = 0, \quad M\psi = h'_0. \quad (\text{F } 3)$$

The relevant null vector for migration is $h'_0 = \partial_1 h$, from which we see that ψ solves the same problem as ψ_1 in equation (3.17). The difference is that (3.17) is determined using the detailed droplet profile rather than the leading order terms in the asymptotic expansions. The solvability conditions that arise in the matched asymptotic analysis therefore yield formulas for the migration dynamics that have the same structure as (3.19). Another solvability condition gives the dynamics of the droplet radii in terms of the flux transmitted across the foot region. This results in mass exchange between droplets as in conventional Ostwald ripening. The net result of all this is to specify the droplet dynamics in terms of flux which arises from quasi-stationary diffusion in the precursor region.

Finally, the matched asymptotic approximation can be further reconnected to the reduced gradient flow of Section 4. An effective medium (Green's function-type) approximation [15, 19] for the exterior Laplace equation in the precursor region can be used to write the dynamics in terms of the droplet radii alone. Such an expansion is valid under the same assumption (4.1) that led to the approximation of the metric coefficients. The sum total of all the formal approximations is a system which resembles the reduced dynamics (e.g. (4.25–4.26)).

References

- [1] ALIKAKOS, N. D., BATES, PETER W. & XINFU CHEN (1994) Convergence of the Cahn–Hilliard equation to the Hele–Shaw model. *Arch. Rational Mech. Anal.* **128**(2), 165–205.
- [2] ALIKAKOS, N. D. & FUSCO, G. (2003) Ostwald ripening for dilute systems under quasistationary dynamics. *Comm. Math. Phys.* **238**(3), 429–479.
- [3] ALIKAKOS, N. D., FUSCO, G. & KARALI, G. (2003) The effect of the geometry of the particle distribution in Ostwald ripening. *Comm. Math. Phys.* **238**(3), 481–488.
- [4] ALIKAKOS, N. D., FUSCO, G. & KARALI, G. (2004) Ostwald ripening in two dimensions – the rigorous derivation of the equations from the Mullins–Sekerka dynamics. *J. Differ. Eq.* **205**(1), 1–49.
- [5] CONSTANTIN, P., DUPONT, T. F., GOLDSTEIN, R. E., KADANOFF, L. P., SHELLEY, M. J. & ZHOU, S.-M. (June 1993) Droplet breakup in a model of the Hele–Shaw cell. *Phys. Rev. E* **47**(6), 4169–4181.
- [6] ELLIOTT, C. M. & GARCKE, H. (1996) On the Cahn–Hilliard equation with degenerate mobility. *SIAM J. Math. Anal.* **27**(2), 404–423.
- [7] GLASNER, K. Ostwald ripening in thin film equations. submitted.
- [8] GLASNER, K. B. & WITELSKI, T. P. (2003) Coarsening dynamics of dewetting films. *Phys. Rev. E* **67**(1), 016302.
- [9] GLASNER, K. B. & WITELSKI, T. P. (2005) Collision versus collapse of droplets in coarsening of dewetting thin films. *Phys. D* **209**(1–4), 80–104.
- [10] GREENSPAN, H. P. (1978) On the motion of a small viscous droplet that wets a surface. *J. Fluid Mech.* **84**, 125–143.
- [11] ONSAGER, L. (1931) Reciprocal relations in irreversible processes, ii. *Phys. Rev.* **38**, 2265.
- [12] ORON, A., DAVIS, S. H. & BANKOFF, S. G. (1997) Long-scale evolution of thin liquid films. *Rev. Mod. Phys.* **69**(3), 931–980.

- [13] OTTO, F., RUMP, T. & SLEPČEV, D. (2006) Coarsening rates for a droplet model: rigorous upper bounds. *SIAM J. Math. Anal.* **38**(2), 503–529 (electronic).
- [14] PEGO, R. L. (1989) Front migration in the nonlinear Cahn–Hilliard equation. *Proc. R. Soc. Lond., Ser. A* **422**(1863), 261–278.
- [15] PISMEN, L. M. & POMEAU, Y. (2004) Mobility and interactions of weakly nonwetting droplets. *Phys. Fluids* **16**(7), 2604–2612.
- [16] PODGORSKI, T., FLESSELLES, J.-M. & LIMAT, L. (2001) Corners, cusps, and pearls in running drops. *Phys. Rev. Lett.* **87**, 036102.
- [17] SEEMANN, R., HERMINGHAUS, S., NETO, C., SCHLAGOWSKI, S., PODZIMEK, D., KONRAD, R., MANTZ, H. & JACOBS, K. (2005) Dynamics and structure formation in thin polymer melt films. *J. Phys.: Condens. Matter* **17**, S267–S290.
- [18] THIELE, U., NEUFFER, K., BESTEHORN, M., POMEAU, Y. & VELARDE, M. (2001) Sliding drops in the diffuse interface model coupled to hydrodynamics. *Phys. Rev. E* **64**, 061601.
- [19] VOORHEES, P. & RATKE, L. (2001) *Growth and Coarsening*. Springer, Berlin.